

# Attribution Quality Metrics with Magnitude Alignment

Chase Walker<sup>1</sup>, Dominic Simon<sup>1</sup>, Kenny Chen<sup>2</sup>, Rickard Ewetz<sup>1</sup>

<sup>1</sup>Department of Electrical and Computer Engineering, University of Central Florida, Orlando, FL, USA

<sup>2</sup>Lockheed Martin, Orlando, FL, USA

{chase.walker, dominic.simon, rickard.ewetz}@ucf.edu, kenny.chen@lmco.com

## Abstract

Attribution algorithms play an instrumental role in human interpretation of AI models. The methods measure the importance of the input features to the model output decision, which can be displayed as an attribution map for image classifiers. Perturbation tests are the state-of-the-art approach to evaluate the quality of an attribution map. Unfortunately, we observe that perturbation tests fail to consider attribution magnitude, which translates into inconsistent quality scores. In this paper, we propose Magnitude Aligned Scoring (MAS), a new attribution quality metric that measures the alignment between the magnitude of the attributions and the model response. In particular, the metric accounts for both the *relative ordering* and the *magnitude* of the pixels within an attribution. In the experimental evaluation, we compare the MAS metric with existing metrics across a wide range of models, datasets, attributions, and evaluations. The results demonstrate that the MAS metric is  $4\times$  more sensitive to attribution changes,  $2\times$  more consistent, and  $1.6\times$  more invariant to baseline modifications. Our code is publicly available via <https://github.com/chasewalker26/Magnitude-Aligned-Scoring>.

## 1 Introduction

Understanding the decision making of black-box AI models is necessary for deployment in safety-critical domains. Attribution methods are currently the most prevalent form of explanations [Das and Rad, 2020]. These methods provide model explanations by assigning an importance value to each feature of the model input [Simonyan *et al.*, 2014]. A broad range of attribution algorithms have been developed in the past few years [Hooker *et al.*, 2019a; Chefer *et al.*, 2021]. However, the ability to quantify the quality of an attribution map remains an open problem. An accurate attribution metric has the potential to further advance the field of explainable AI forward, refining human understanding of AI models.

Attribution quality metrics generally fall into two categories: evaluation with ground-truth [Borji *et al.*, 2013] or perturbation metrics without ground-truth [Samek *et al.*,

2016; Ancona *et al.*, 2018]. Evaluation of attribution methods with ground-truth can be desirable when human-labeled data is present. Common methods to develop ground-truth datasets in the vision domain are the use of segmentation algorithms to create a mask of the image subject, human eye-tracking heat map data, or manual image masks created by humans [Kümmerer *et al.*, 2014; Bylinskii *et al.*, 2019]. Perturbation metrics aim to quantify the quality of an attribution map without the use of ground-truths that are often not available [Samek *et al.*, 2016]. Moreover, human-created masks do not necessarily represent a model’s decision process.

Perturbation metrics aim to evaluate if the attribution map is reflective of a model’s decision making [Petsiuk *et al.*, 2018b]. Specifically, perturbation tests aim to measure if the attribution map discriminates appropriately between more and less important features. The tests are performed by modifying the model or the input test image by the values in the attribution map [Petsiuk *et al.*, 2018b]. Ideally, *the magnitude of the attribution assigned to each feature should be proportional to the model response*. However, we observe that current image perturbation metrics do not measure this relationship, they only account for the relative ordering of the input features, not the magnitudes, leading to inconsistent scores.

In this paper, we propose a new perturbation metric for evaluating attribution quality without ground-truth called Magnitude Aligned Scoring (MAS). MAS employs an *alignment penalty* to measure the relationship between attribution magnitude and the response of the model output to the attribution. Our main contributions can be summarized as follows:

- We observe that existing quality metrics fail to consider attribution magnitude and only rely on attribution order, which leads to inconsistent quantification.
- We propose a quantitative, ground-truth-free perturbation metric, MAS. It provides a principled solution to the failures of existing methods by utilizing an *alignment penalty* to satisfy a new *sensitivity* property we define.
- Quantitative analysis proves MAS solves the failures of existing metrics, showing  $2.5\times$  improvements across sensitivity, consistency, and baseline invariance testing.

The paper is arranged as follows: related work is discussed in Section 2, the MAS metric is motivated in Section 3, the MAS metric is defined in Section 4, experimental evaluation is performed in Section 5, and the conclusion is in Section 6.

## 2 Related Work

In this section, we discuss the details of attribution methods, the existing metrics that quantify their accuracy, and how these metrics can be validated.

### 2.1 Attribution Methods

Attribution methods explain black-box models by measuring the importance of each feature in an input to the model response. Attribution methods can be occlusion based [Ribeiro *et al.*, 2016; Zeiler and Fergus, 2014], gradient based [Simonyan *et al.*, 2014], or attention based methods [Hao *et al.*, 2021] for transformer models. Occlusion based methods iteratively modify an input image while measuring model output to determine the most salient regions. Gradient based methods use backpropagation to measure the model gradients with respect to the input features. Attention based methods use transformer attention weights as explanations directly, or combine them with model gradients [Yuan *et al.*, 2021]. Occlusion based methods are slow and generally undesirable.

The early gradient based techniques utilize model gradients as is [Simonyan *et al.*, 2014] or multiply them by the input image [Shrikumar *et al.*, 2016], but these methods suffer from large amounts of saturation noise [Sundararajan *et al.*, 2017]. Recently, the newly introduced path integration methods [Miglani *et al.*, 2020] average the gradients from multiple interpolated images along a path from a baseline to the input image to reduce this saturation noise. Additional techniques to reduce noise suppress negative gradients during the backpropagation step [Springenberg *et al.*, 2015] or measure gradients from a models’ last convolutional layer and remove gradients pointing to non-target classes [Selvaraju *et al.*, 2017]. Attention based methods first started with raw attention as a visualization [Hao *et al.*, 2021] and have since incorporated accumulation techniques [Yuan *et al.*, 2021; Chefer *et al.*, 2021] and gradients [Qiang *et al.*, 2022] to create stronger attributions. Attribution metrics are necessary to measure how well an attribution represents a model.

### 2.2 Attribution Quality Metrics

Attribution quality metrics aim to evaluate how well an attribution represents a model’s decision making process. We focus on improving perturbation metrics because ground-truths are generally not available. Within perturbation metrics, there are methods that perturb [Adebayo *et al.*, 2018] or retrain a model [Hooker *et al.*, 2019b] and those that perturb the input and retain the original model [Petsiuk *et al.*, 2018b]. These model modification metrics either randomize model layers and measure how much an attribution changes [Adebayo *et al.*, 2018], or retrain a model with the top attribution pixels ablated from the train set [Hooker *et al.*, 2019b]. Since these methods require data intensive and model-specific retraining or modification, we will focus on image perturbation metrics for this work [Petsiuk *et al.*, 2018b].

Image perturbation metrics exist as insertion or deletion tests and use the original image, an attribution, a baseline (blurred starting image for insertion or black ending image for deletion), and the model. In insertion (deletion) testing, original (black) pixels are iteratively added to the blurred (original) input image in order of descending attribution magnitude

until the original (a black) image is reached. The model output is measured for the perturbed image at each iteration with respect to the original class, resulting in a receiver operating characteristics (ROC) curve. For insertion (deletion) tests, this is an increasing (decreasing) curve and the area under the ROC curve - the AUC - gives the final result, where a higher (lower) value represents a better attribution. This traditional ROC curve is visualized in Figure 2(b) for the insertion test. It is most common for the results of both the insertion and deletion tests to be presented for the evaluation of an attribution. In this work we evaluate two methods which follow this perturbation process.

**RISE: Insertion and Deletion** In the RISE paper [Petsiuk *et al.*, 2018b], the authors use the standard baselines for the insertion and deletion tests (the blurred input or black image), and use equally sized pixel groupings during the testing process. At each perturbation step, they select the top  $N$  pixels of an  $N \times N$  image by descending attribution magnitude and measure the resulting softmax output to generate an ROC.

**PIC: SIC and AIC Insertion** Kapishnikov *et al.* present the performance information curve (PIC) insertion metrics: the softmax information curve (SIC) and accuracy information curve (AIC) scores [Kapishnikov *et al.*, 2019]. SIC uses the softmax output, whereas AIC uses an accuracy measurement of 0 or 1 for an incorrect or correct prediction at each perturbation step. Instead of a uniform blur baseline, the input image is blurred in discrete, polygonal tiles, with unique noise distributions. Additionally, pixels are non-linearly perturbed in groups of increasing size, and the SIC/AIC ROCs are normalized to be monotonic non-decreasing curves.

### 2.3 Desirable Attribution Metric Properties

A trustworthy and reliable attribution quality metric should adhere to the following desirable properties which are quantitatively measurable:

1. **Sensitivity:** Features important to the model should have high attribution and unimportant features should have low attribution [Petsiuk *et al.*, 2018b].
2. **Consistency:** A metric should be consistent in its calculated ratings. It should consistently rank different attribution methods by their quality over a set of varying inputs [Tomsett *et al.*, 2020].
3. **Baseline Invariance:** A metric should be invariant to its baseline selection, i.e., an insertion test using a random baseline or blurred baseline should rank a set of attributions the same way [Tomsett *et al.*, 2020].

Existing image perturbation metrics attempt to satisfy sensitivity by scoring attributions using the relative ordering of the input features. However, the sensitivity property is rather vaguely defined, so it is not clear which one of the RISE and PIC metrics best quantifies the property. Hence, a mix of the different tests are typically used to evaluate new attribution algorithms. Additionally, it has been shown that consistency and baseline invariance are not adequately satisfied by the RISE and PIC methods [Tomsett *et al.*, 2020].

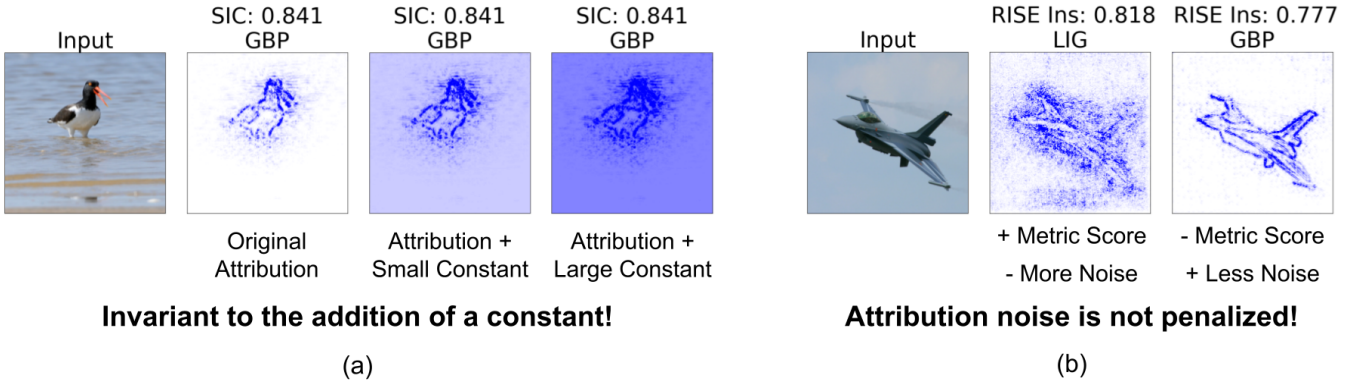


Figure 1: (a) Adding a constant to the GBP “oystercatcher” attribution does not affect the SIC score. The explanation is that the SIC metric only accounts for the (unchanged) attribution order and not attribution magnitudes. (b) RISE insertion scores the “warplane” LIG attribution higher than GBP although GBP provides a sharper version of the LIG attribution with less saturation noise. This is explained by the fact that there does not exist a penalty for attributions on unimportant features in the existing metrics as attribution magnitude is not considered.

### 3 Motivating a New Metric

We now study the RISE and PIC metrics to show their failure of sensitivity resulting from their disregard of attribution magnitude and motivate the definition of a new sensitivity property as well as the development of a new metric.

#### 3.1 Attribution Magnitude is Important

In Section 2.3, the sensitivity property states that input pixels that are important (not important) to the model’s decision should be assigned large (small) magnitude attributions. Here, small and large refers to the relative distance to zero. Formally, let  $A_i$  and  $A_j$  denote the attributions of pixels  $i$  and  $j$ , respectively. The quotient  $A_i/A_j$  measures the relationship of the features’ magnitudes, which defines sensitivity.

Given this notation, we analyze the invariance of attribution metrics to multiplying an attribution map by a constant or adding a constant. It is straightforward to understand that invariance to multiplication is desirable for a metric, as  $A_i/A_j$  is equal to  $aA_i/aA_j$ , where  $a$  is a constant. However,  $(A_i + a)/(A_j + a)$  is not equal to  $A_i/A_j$ , in general. Therefore, invariance to a constant offset is undesirable under the sensitivity property, but existing metrics do not adhere to this.

#### 3.2 Limitations of State of the Art Metrics

##### Increase by a Constant Is Ignored

In Figure 1(a), we modify guided backpropagation (GBP) [Springenberg *et al.*, 2015] attributions by adding 5% or  $10\% \times \max(\text{GBP})$  to all attribution pixels as a constant. Since *adding a constant does not change the relative ordering of the input features*, the attribution maps are scored equally by SIC. This holds for all four reviewed metrics - RISE insertion and deletion as well as PIC’s SIC and AIC. Thus, it is clear the existing attribution metrics’ sole reliance on relative attribution ordering leads to an invariance to a constant offset.

**Theorem 1.** *RISE and PIC Are Invariant to Constant Offset.*

*Proof.* Let an attribution  $A$  with values in the range  $[0, 1]$  have a magnitude ordering of  $O_A$ . If a constant  $b$  is added to  $A$ , this yields  $A'$ , with range  $[b, 1+b]$  and ordering  $O_{A'} =$

$O_A$ . Since a score is determined solely by the perturbation of the input image via the order of  $A$ , and  $O_A = O_{A'}$ ,  $A$  and  $A'$  will have equal scores. Therefore, the metrics are invariant to a constant offset.  $\square$

##### Attribution Noise Is Not Penalized

We show the attribution maps of a “warplane” image computed using left integrated gradients (LIG) [Miglani *et al.*, 2020] and GBP in Figure 1(b). Although GBP has a very sharp, low noise attribution compared to LIG, which has evident saturation noise [Sundararajan *et al.*, 2017], the RISE insertion metric scores LIG higher than GBP. Given the attributions are nearly identical except for the noise in LIG, it is clear that existing metrics do not sufficiently penalize non-zero attributions on unimportant input features. This is a direct result of not adhering to the sensitivity property.

#### 3.3 Proportional Sensitivity

In this paper, we propose a quantitatively satisfiable property in replacement of the vaguely defined sensitivity property:

1. **Proportional Sensitivity:** *The magnitude of the attribution assigned to an input feature should be directly proportional to the change the feature induces in the model output response.*

To satisfy this property, we propose a new metric that penalizes the misalignment of an attribution feature’s model response and density response. This encourages large magnitude attributions to be assigned to the critical input features while penalizing non-zero attributions assigned to pixels that are irrelevant to the model. We envision this new metric will drive the development of new attribution algorithms that produce sharp, low noise attribution maps.

### 4 The MAS Metric

In this section, we introduce the magnitude aligned scoring (MAS) metric. We define the model and density response to introduce an *alignment penalty* that satisfies the proportional sensitivity property. The model response measures a feature’s proportional contribution to the model output and the density

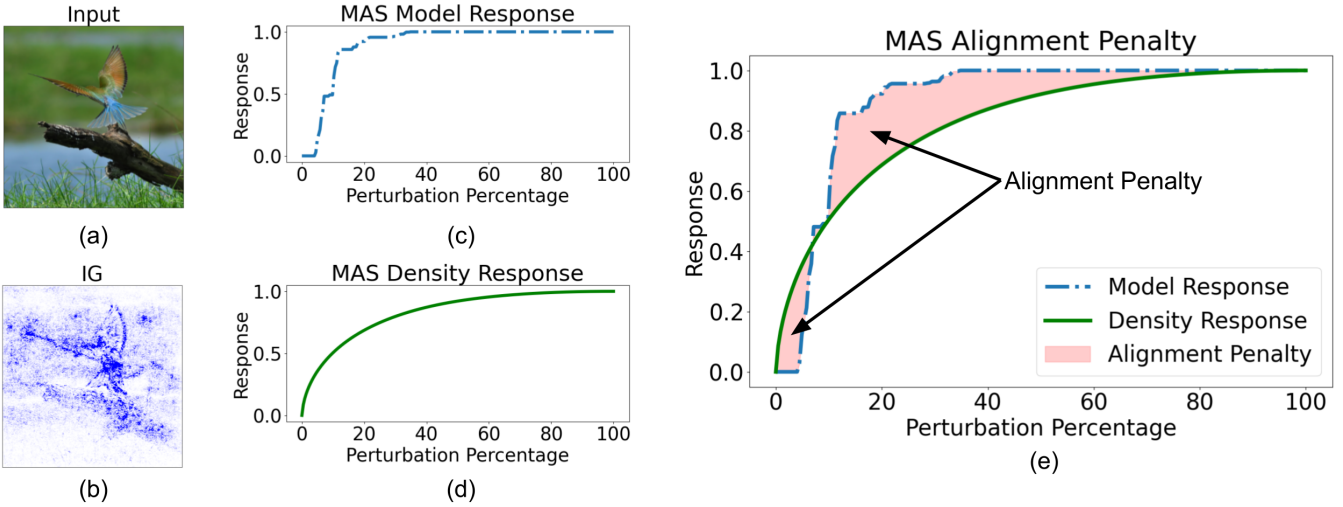


Figure 2: This figure outlines the process for computing the model response, density response, and alignment penalty of our new MAS insertion test given an image and its attribution map. For the input image of a “bee eater” (a) and its IG attribution map (b), we show the model response (c), density response (d), and alignment penalty (e) as the area between the response curves.

response measures a feature’s proportional contribution to the entire attribution’s magnitude. Figure 2 provides an overview.

#### 4.1 The Model and Density Response

Given an input  $X$  of class  $c$ , a model  $F$ , and an attribution map  $A$ ,  $N$  attribution features are evaluated over an  $N$  step perturbation test. For a step  $k$ , the perturbed image  $X_k$  evaluates the impact of the first  $k$  attribution features in highest magnitude order. This test follows the RISE process from Section 2.2. We define the model response ( $MR$ ) at step  $k$  as:

$$MR_k = \text{softmax}(F(X_k))_c, \quad (1)$$

where  $X_0$  represents the unperturbed starting image and  $MR_0$  to  $MR_N$  forms the  $MR$  curve. In Figure 2, we show an input image of a “bee eater” (a), its integrated gradients (IG) [Sundararajan *et al.*, 2017] attribution map (b), and the model response (c) from an MAS insertion test. We note that the insertion model response  $MR^{\text{ins}}$  is a monotonically *increasing* curve, and  $MR^{\text{del}}$  is a monotonically *decreasing* curve.

Next, we define the density response ( $DR$ ) at step  $k$  as:

$$DR_k = \frac{\sum_{i=0}^k |A_i|}{|A|} \quad (2)$$

where the  $|.|$  operation measures the total magnitude of the attributions in a given feature,  $A_0$  represents 0 selected features, and  $DR_0$  to  $DR_N$  forms a full density response curve. The density response of the “bee eater” IG attribution is seen in Figure 2(d) and represents, at each step, what percentage of the total attribution magnitude has been selected via the perturbation process. We note that the insertion model response  $DR^{\text{ins}}$  is a monotonically *increasing* curve, and  $DR^{\text{del}} = 1 - DR^{\text{ins}}$  is a monotonically *decreasing* curve.

Now we define the alignment penalty ( $AP$ ) which measures the absolute value of the difference between the model and density response for an attribution map. The general

alignment penalty at step  $k$  is defined as:

$$AP_k = |MR_k - DR_k|, \quad (3)$$

where  $AP_0$  to  $AP_N$  measures the alignment penalty across the full insertion or deletion  $MR$  and  $DR$  curves. In Figure 2(e), the insertion alignment penalty is illustrated as the area between the  $MR$  and  $DR$  curves.

#### 4.2 Magnitude Aligned Scoring (MAS)

Given an attribution map  $A$  with  $N$  features, MAS can be utilized as insertion or deletion. The insertion and deletion tests are defined by the AUC of the  $MR$  and  $AP$  curves:

$$\text{MAS}^{\text{ins}} = \frac{1}{N} \sum_{i=0}^N MR_i^{\text{ins}} - \frac{1}{N} \sum_{i=0}^N AP_i^{\text{ins}} \quad (4)$$

and

$$\text{MAS}^{\text{del}} = \frac{1}{N} \sum_{i=0}^N MR_i^{\text{del}} + \frac{1}{N} \sum_{i=0}^N AP_i^{\text{del}}. \quad (5)$$

Intuitively, lowering (increasing) the insertion (deletion) score is the effective application of the alignment penalty because a higher (lower) insertion (deletion) score represents a higher quality attribution.

To calculate the  $MR$ , we perform the linear perturbation process from RISE explained in Section 2.2 and we perform monotonic normalization of the  $MR$  to  $[0, 1]$  to ensure  $AP = 0$  is achievable as  $DR$  is on the range  $[0, 1]$ . The penalized  $\text{MAS}_{\text{ins}}$  or  $\text{MAS}_{\text{del}}$  ROC is then clipped to the range  $[0, 1]$  and normalized to  $[0, 1]$ . Therefore, the AUC of the resulting  $\text{MAS}^{\text{ins}}$  and  $\text{MAS}^{\text{del}}$  scores is on the range  $[0, 1]$  where higher is better for  $\text{MAS}^{\text{ins}}$  and lower for  $\text{MAS}^{\text{del}}$ .

We present how the MAS insertion test accounts for attribution magnitude in Figure 3 by revisiting the LIG and GBP attributions of the “warplane” seen in Figure 1(b). From left to right, we show the input (a), an attribution, its  $MR$ ,  $DR$ ,

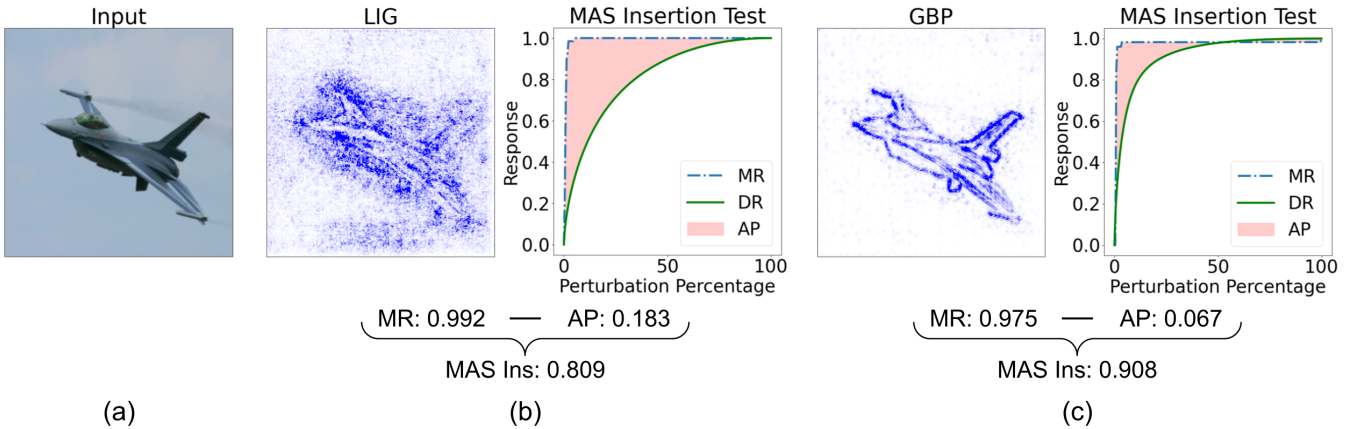


Figure 3: The calculation of the MAS insertion scores for (b) LIG and (c) GBP attributions of a “warplane” (a). Each graph shows the  $MR$ ,  $DR$ , and  $AP$ . It can be seen LIG has a model response with a higher AUC than GBP (since magnitude is not a factor), but receives a much larger alignment penalty when noise is considered, resulting in a lower score than GBP, as expected. The alignment penalty therefore corrects the non-penalization of attribution noise by the existing methods.

and  $AP$  graph, and its MAS score calculation beneath. In Figure 3(b) we see LIG has a large model response of 0.992 which is greater than GBP’s model response of 0.975 in Figure 3(c) (since magnitude is not a factor without the alignment penalty). However, due to the noise in the LIG attribution, it has a large alignment penalty of 0.183 compared to 0.067 for GBP. When the  $AP$  is subtracted from the  $MR$  of each attribution, the final scores are 0.809 and 0.908 for LIG and GBP, respectively. The proper penalization of noise in the LIG attribution results in a lower score than GBP, as expected.

**Insertion and Deletion Difference** In the existing literature, insertion and deletion tests are often performed in unison, but considered separately as they measure different qualities of an attribution. The insertion test measures the value of high magnitude attributions to classification by adding them to an image, while the deletion test measures the value of high magnitude attributions to misclassification by removing them from an image. However, we propose a combination of the scores should also be considered to balance the bias of each test. We propose considering the difference of the scores:

$$MAS^{\text{diff}} = MAS^{\text{ins}} - MAS^{\text{del}}. \quad (6)$$

The subtraction of these two tests creates the new “difference” score while preserving their opposing nature: higher insertion scores and lower deletion scores are desired. If one score measures very well and one very poorly, the small difference will indicate the disagreement between the tests (one test is biased). If both scores are respectively strong, the large difference will indicate an overall high scoring attribution.

### 4.3 MAS Is Sensitive to a Constant Offset

**Theorem 2.** *MAS is sensitive to a constant offset.*

*Proof.* The MAS score of an attribution  $A$  is defined as:

$$MAS(A) = MR - |MR - DR|, \quad (7)$$

where  $MR$  is equivalent to the score of the RISE metrics. Following Proof (3.2), if  $MAS(A)$  and  $MAS(A')$  are evaluated, the  $MR$  terms of each function will be equivalent.

So we write  $MAS = f(DR)$ . Now, consider  $A \in [0, 1]$  and  $A' \in [b, 1 + b]$ . By Eq (2),  $DR(A) \neq DR(A')$ , thus  $MAS(A) \neq MAS(A')$ , proving MAS is sensitive to a constant offset, satisfying proportional sensitivity.  $\square$

## 5 Evaluation

We perform evaluation of the proposed MAS metrics against the currently accepted PIC [Kapishnikov *et al.*, 2019] and RISE [Petsiuk *et al.*, 2018b] perturbation metrics for a total of eight metrics under evaluation: AIC, SIC, RISE insertion, RISE deletion, RISE difference, MAS insertion, MAS deletion, and MAS difference. We recognize difference was not employed in the original RISE framework, but we use it for fair comparison against our proposed MAS difference metric.

All evaluations are performed with PyTorch [Paszke *et al.*, 2019], using ResNet 101 (R101) [He *et al.*, 2016] and ViT-Base 16 (ViT16) [Dosovitskiy *et al.*, 2020]. The evaluations are executed on an internal cluster with NVIDIA A40 GPUs. We employ the Imagenet [Russakovsky *et al.*, 2015] and RE-SISC45 [Cheng *et al.*, 2017] datasets across our experiments. We use the respective repositories of the PIC [Kapishnikov *et al.*, 2021b] and RISE [Petsiuk *et al.*, 2018a] metrics.

### 5.1 Metric Attribution Sensitivity Test

As presented in Figure 1(a) and (b), the RISE and PIC metrics do not recognize a constant offset or properly penalize attribution noise because they do not consider attribution magnitude, and therefore are not *sensitive* as outlined in Section 2.3. We now quantitatively verify MAS’ sensitivity.

Using the ImageNet and RESISC45 datasets with the R101 and ViT16 models, we generate gradient (grad) [Simonyan *et al.*, 2014], LIG, and GBP attributions for 1000 images from both datasets. We choose these attribution methods for their different levels of noise. We then perform one of two modifications to the generated attributions. We either add a constant that is 5, 10, 25, or 50% of the maximum attribution value as explained for Figure 1(a) or we add noise from the range 0 to 0.05, 1, 2, or 3% of the maximum attribution value.

Noise Type	Constant Offset				Noised			
	ImageNet		RESISC 45		ImageNet		RESISC 45	
Dataset	R101	VIT16	R101	VIT16	R101	VIT16	R101	VIT16
PIC: SIC [Kapishnikov <i>et al.</i> , 2019] ( $\uparrow$ )	0.00	0.00	0.00	0.00	2.63	0.89	0.46	0.74
PIC: AIC [Kapishnikov <i>et al.</i> , 2019] ( $\uparrow$ )	0.00	0.00	0.00	0.00	2.80	0.88	0.74	0.55
RISE Ins [Petsiuk <i>et al.</i> , 2018b] ( $\uparrow$ )	0.00	0.00	0.00	0.00	14.17	3.43	1.51	3.77
RISE Del [Petsiuk <i>et al.</i> , 2018b] ( $\uparrow$ )	0.00	0.00	0.00	0.00	4.99	3.88	2.39	1.55
RISE Diff [Petsiuk <i>et al.</i> , 2018b] ( $\uparrow$ )	0.00	0.00	0.00	0.00	8.94	2.28	1.80	2.68
MAS Ins (ours) ( $\uparrow$ )	<b>20.41</b>	<b>20.21</b>	<b>25.08</b>	<b>27.51</b>	<b>14.65</b>	<b>9.84</b>	<b>11.60</b>	<b>18.16</b>
MAS Del (ours) ( $\uparrow$ )	<b>23.39</b>	<b>21.10</b>	<b>25.43</b>	<b>27.10</b>	<b>12.18</b>	<b>4.00</b>	<b>12.92</b>	<b>14.02</b>
MAS Diff (ours) ( $\uparrow$ )	<b>22.02</b>	<b>20.67</b>	<b>25.25</b>	<b>27.31</b>	<b>13.32</b>	<b>6.86</b>	<b>12.25</b>	<b>16.12</b>

Table 1: We evaluate the sensitivity of each metric. The values measure how sensitive each metric is to attribution modification (a constant offset of all values or a noised version of the attribution), where higher is better. Across all tests, MAS has greatly improved sensitivity.

Dataset	ImageNet		RESISC 45	
	Model	R101	VIT16	R101
PIC: SIC [Kapishnikov <i>et al.</i> , 2019] ( $\uparrow$ )	0.323	0.262	0.025	0.268
PIC: AIC [Kapishnikov <i>et al.</i> , 2019] ( $\uparrow$ )	0.185	0.263	0.017	<b>0.382</b>
RISE Ins [Petsiuk <i>et al.</i> , 2018b] ( $\uparrow$ )	0.479	0.128	0.015	0.056
RISE Del [Petsiuk <i>et al.</i> , 2018b] ( $\uparrow$ )	0.378	0.330	0.181	0.117
RISE Diff [Petsiuk <i>et al.</i> , 2018b] ( $\uparrow$ )	0.657	0.448	0.071	0.162
MAS Ins (ours) ( $\uparrow$ )	<b>0.634</b>	<b>0.491</b>	<b>0.158</b>	0.259
MAS Del (ours) ( $\uparrow$ )	<b>0.678</b>	<b>0.669</b>	<b>0.497</b>	<b>0.500</b>
MAS Diff (ours) ( $\uparrow$ )	<b>0.715</b>	<b>0.650</b>	<b>0.237</b>	<b>0.387</b>

Table 2: We evaluate the ability of each metric to be consistent in its ordering of a set of attributions over a set of images. A more consistent metric is more trustworthy. We measure this consistency with the IRR metric, where a higher value is better.

We then average, over the images, the ROCs computed by each of the eight metrics for all attributions and their modifications. We then measure the absolute distance of the modified attribution ROCs from the original ROC. We evaluate a metric’s sensitivity by the ratio of the distance metric to the original attribution’s AUC. A sensitive metric will have a non-zero ratio value, where higher indicates more sensitivity.

In Table 1, we see only MAS is sensitive to a constant offset and MAS outperforms PIC and RISE in all noised sensitivity tests. MAS is overall more sensitive to changes in an attribution as it considers attribution magnitude via the alignment penalty. In Section A.1, we present the ROC curves from the table that show MAS reduces the score of the modified (worse) attributions, whereas PIC and RISE do not consistently increase or decrease the score if the score changes.

## 5.2 Metric Ranking Consistency Test

To evaluate the *consistency* of how a metric rates a group of attributions, we perform two metric sanity checks [Tomsett *et al.*, 2020]: inter-rater reliability (IRR) and internal consistency reliability (ICR). IRR measures how well a metric sorts a set of attributions over a set of images. A perfectly *consistent* metric is expected to provide the same ordering of an attribution set over all images. Krippendorff’s  $\alpha$  is used to measure the IRR of a metric [Krippendorff, 2004], where a

higher  $\alpha$  in the range  $[0, 1]$  represents a more consistent metric. We provide the ICR results in Appendix A.2.

We measure the IRR of the eight metrics using three attributions over 5000 images from the ImageNet and RESISC45 datasets. For the R101 model, we select the grad, LIG, and GBP attributions due to their large visual differences (see Figure 4). For the VIT16 model, we select the following attribution group: a random mask, LIG, and transition attention [Yuan *et al.*, 2021] or raw attention [Hao *et al.*, 2021] for ImageNet and RESISC45, respectively, due to their large visual differences. These were chosen as visually similar attributions are likely to be scored equivalently, making consistent ranking unlikely for any metric. The IRR test results are in

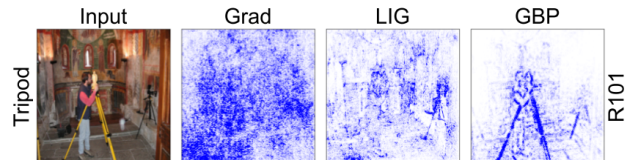


Figure 4: The attributions, sorted low to high by score, chosen for ImageNet using R101. Note the differences in pixel distribution and density of the attribution maps. In MAS testing, grad consistently scores worse than LIG, which consistently scores worse than GBP.

Baseline	Random								Dataset Mean	
	Dataset		ImageNet		RESISC 45		ImageNet		RESISC 45	
Model	R101	VIT16	R101	VIT16	R101	VIT16	R101	VIT16	R101	VIT16
RISE Ins [Petsiuk <i>et al.</i> , 2018b] ( $\uparrow$ )	0.495	0.331	0.056	0.177	0.505	0.312	0.052	0.174		
RISE Del [Petsiuk <i>et al.</i> , 2018b] ( $\uparrow$ )	0.369	0.235	0.131	0.052	0.368	0.247	0.157	0.045		
RISE Diff [Petsiuk <i>et al.</i> , 2018b] ( $\uparrow$ )	0.600	0.537	0.131	0.267	0.610	0.550	0.149	0.265		
MAS Ins (ours) ( $\uparrow$ )	<b>0.554</b>	<b>0.463</b>	<b>0.160</b>	<b>0.287</b>	<b>0.554</b>	<b>0.463</b>	<b>0.166</b>	<b>0.283</b>		
MAS Del (ours) ( $\uparrow$ )	<b>0.680</b>	<b>0.631</b>	<b>0.466</b>	<b>0.496</b>	<b>0.680</b>	<b>0.631</b>	<b>0.490</b>	<b>0.477</b>		
MAS Diff (ours) ( $\uparrow$ )	<b>0.660</b>	<b>0.606</b>	<b>0.296</b>	<b>0.430</b>	<b>0.674</b>	<b>0.606</b>	<b>0.319</b>	<b>0.419</b>		

Table 3: We measure how invariant a metric’s consistency is under baseline modification. It is ideal for a metric to be implementation invariant such that it provides more accurate results. We measure the invariance with the ICR metric where higher values are better.

Table 2 where MAS shows a significantly higher consistency than the RISE and PIC metrics, outperforming them in 11/12 tests. We illustrate the consistency improvements of MAS with Figure 5 and figures in Appendix A.2.

### 5.3 Metric Baseline Invariance Test

As explained in Section 2.3, it is desirable for a quality metric to consistently evaluate attributions *regardless of its baseline*. ICR measures how well two different metrics agree on attribution rankings via Spearman’s  $\rho \in [0, 1]$ , where a higher value represents stronger agreement. We evaluate the agreement of the six RISE and MAS quality metrics with their modified baseline versions. We exclude PIC due to inaccessibility of modification. We use either random values drawn from a uniform distribution or the dataset mean value as the new baseline [Tomsett *et al.*, 2020]. The default baseline for insertion is a blurred image and for deletion, a black image. We use the same image, model, and attribution choices from the previous section for evaluation. The results in Table 3 show that MAS is more invariant to baseline modification than RISE in 24/24 tests, as desired. A visual explanation of this test is provided with a figure in Appendix A.3.

### 5.4 Qualitative Analysis of MAS

To qualitatively verify MAS against PIC and RISE, we provide ten examples in Appendix A.4 and one in Figure 5. We score seven attributions: IG, LIG, GBP, GradCAM and guided GradCAM [Selvaraju *et al.*, 2017], guided IG (GIG) [Kapishnikov *et al.*, 2021a], and adversarial gradient integration (AGI) [Pan *et al.*, 2021] using the eight tests discussed in this paper. This figure evaluates the properties of sensitivity and consistency. Observing the location of noisy attributions in the orderings, MAS shows greatly improved sensitivity by placing noisy attributions at the worst ranks across all three metrics, whereas RISE and PIC fail to do so. The figure also shows that the RISE and PIC tests do not sort consistently compared to MAS which is consistent in ranks 1 - 4 and 7.

## 6 Conclusion

We discover that current state-of-the-art attribution quality metrics fail to consider attribution magnitude which leads to poor quantification as they fail invariance properties.

Through the introduction of the *alignment penalty* to account for the relationship between attribution magnitude and model response, we define the MAS framework which properly evaluates attributions. We show quantitatively that the MAS metrics, unlike the existing state-of-the-art metrics, satisfy the three desired properties of attribution quality metrics: sensitivity, consistency, and invariance to baseline selection. This greatly improves the ability of a user to select a desired, high-performance attribution method. We believe MAS will be used to develop high-quality attribution methods. In future work, we intend to use the alignment penalty to refine existing attributions by removing unimportant features.

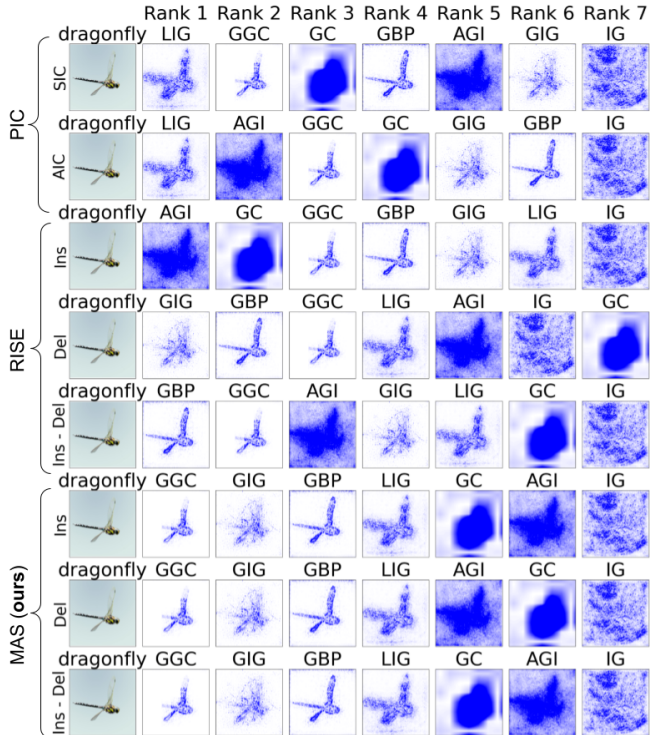


Figure 5: A visualization of the metric attribution sorting comparison (IRR) from Section 5.2. It is clear that MAS sorts most consistently with improved sensitivity (low noise attributions first).

## A Appendix

This appendix provides additional details which did not fit in the main paper. In Appendix A.1 we present figures of the ROC curves that were used in Table 1 of the paper. In Appendix A.2 we use figures to explain the tests performed for Table 2 of the main paper and present the ICR consistency test results. In Appendix A.3 we show the baseline changes for the metrics from Table 3 of the main paper. In Appendix A.4 we present ten additional figures like Figure 5 from the main paper. In Appendix A.5 we explain code details and provide a URL.

### A.1 Extended Metric Attribution Sensitivity Test

We present figures which display the ROC curves that were generated for the sensitivity measurement test. There are eight figures 6 to 13, on pages 2 to 5, which cover the tests. We tested two types of attribution modifications: increase by a constant and noising, for both the ImageNet and RESISC45 datasets, and the R101 and VIT16 models. Each figure covers one combination of these three options. The first four show constant offset results and last four show noised results.

For example, Figure 6 shows the PIC, RISE and the MAS metric curves for the constant offset sensitivity test using ImageNet and R101. It is clear to see for this figure and the next three constant offset figures, that only MAS can detect the modification. In addition to this, it is clear that MAS always penalizes these modifications as the curves get worse for their respective test types (insertion and difference curves have less AUC, and deletion has more AUC). In the noised sensitivity figures, we see again that MAS always penalizes the scores, whereas PIC and RISE tests will at times reward the noised attributions with respect to the original.

### A.2 Extended Metric Ranking Consistency Test

We first show nine comparisons of RISE and MAS consistency to illustrate MAS’ improvements. Next, we present the ICR consistency test results as referenced in the paper.

#### IRR RISE vs MAS Ranking

As seen in Table 1, the MAS metrics are significantly more consistent than the RISE tests. This is due to the use of the alignment penalty in the MAS metrics. We compare 9 examples in Figure 14, on page 13, to show how the inclusion of the alignment penalty changes the orderings provided by RISE insertion to the orderings provided by MAS insertion. It is clear that RISE, on the left side, is not consistent across images, but when the alignment penalty is added - by using MAS - we see improved consistency and sensitivity.

#### ICR Framework Ranking Consistency

We use ICR to compare the agreement of the two metrics in each framework: AIC and SIC for PIC, and insertion and deletion for RISE and MAS. The ICR results are presented in Table 4 for the same data, models, and attributions as the IRR tests. The MAS framework is more consistent than PIC and RISE in every test. Interestingly, the PIC metrics agree less than MAS although both are insertion and could be expected to strongly agree. Also, the RISE tests do not greatly agree (they measure separate concepts as discussed in the main paper), but MAS has greatly improved agreement.

Dataset	ImageNet		RESISC 45		
	Model	R101	VIT16	R101	VIT16
PIC [2019] ( $\uparrow$ )		0.249	0.262	0.021	0.322
RISE [2018b] ( $\uparrow$ )		0.422	0.207	0.066	0.083
MAS (ours) ( $\uparrow$ )		<b>0.652</b>	<b>0.574</b>	<b>0.295</b>	<b>0.369</b>

Table 4: We evaluate framework consistency by comparing the internal agreement of their respective metrics. We measure this consistency with the ICR metric, where a higher value is better.

### A.3 Extended Metric Baseline Invariance Test

In Figure 15, on page 14, we show the baseline modifications from Table 3. Insertion’s default (a) moves from a blurred baseline image to the input. Deletion’s default (b) moves from the input to a black baseline. The modified baselines (c) are either random noise or the dataset mean.

### A.4 Extended Qualitative Analysis of MAS

With Figures 16 to 25, on pages 15 to 24, we provide ten examples to further show that MAS outperforms PIC and RISE in sensitivity (low noise attributions first) and consistency.

### A.5 Code Details

All parameter details are included with the code database. Default parameters are used from their respective sources (referenced in the code) for all methods. <https://github.com/chasewalker26/Magnitude-Aligned-Scoring>.

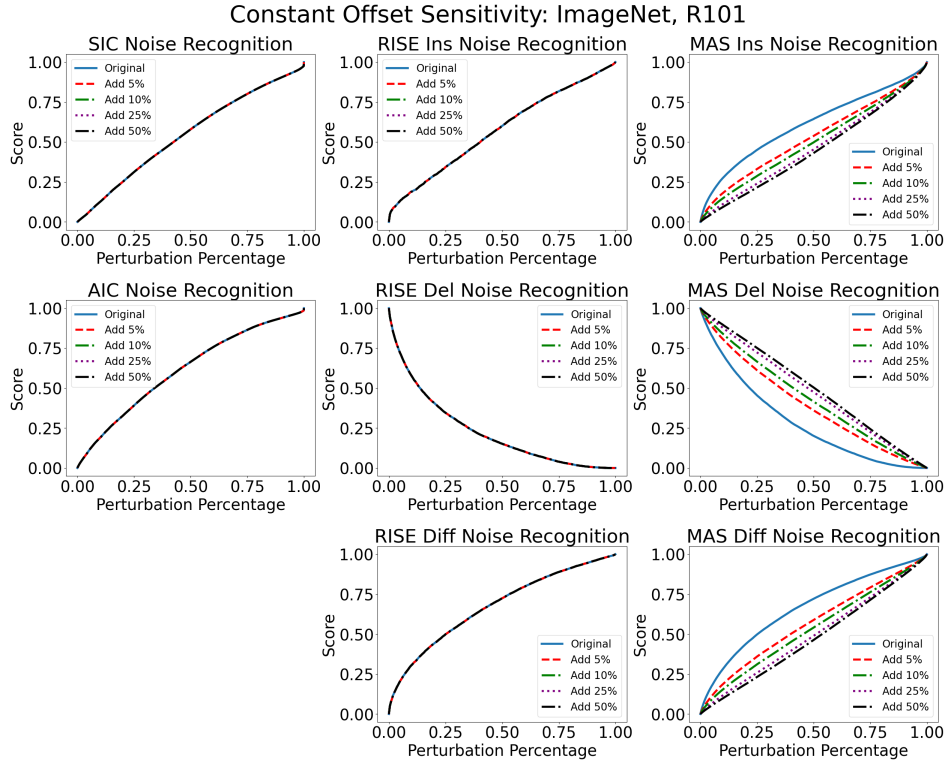


Figure 6: The ROC curves from the constant offset sensitivity test for the ImageNet dataset and R101 model. MAC is seen to be sensitive to the constant offset, while PIC and RISE cannot recognize the constant offset.

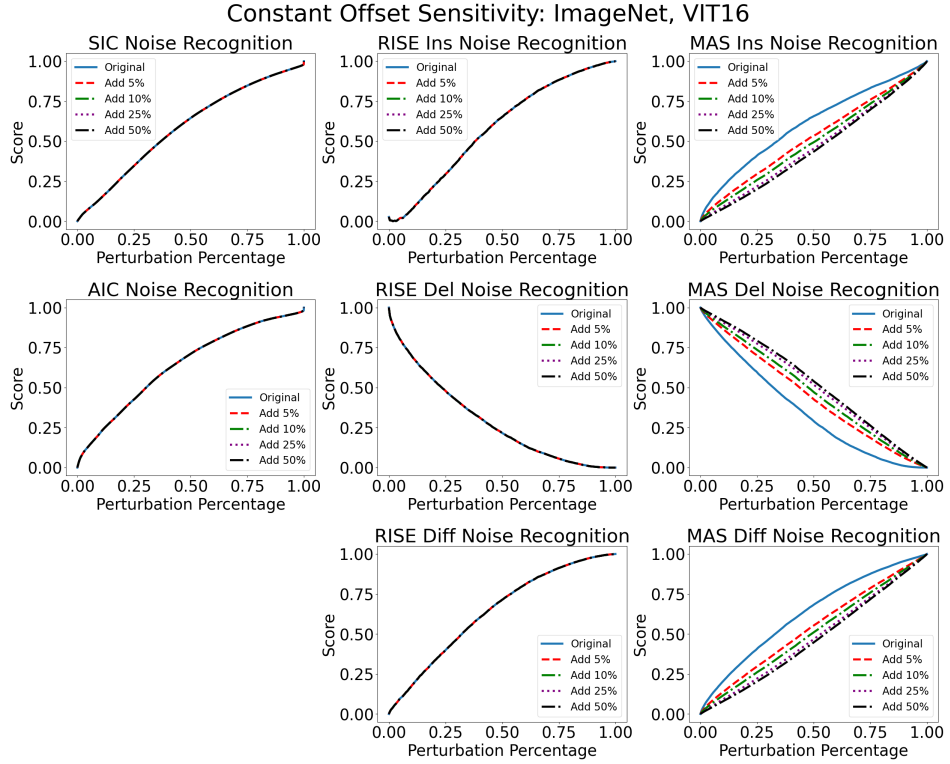


Figure 7: The ROC curves from the constant offset sensitivity test for the ImageNet dataset and VIT16 model. MAC is seen to be sensitive to the constant offset, while PIC and RISE cannot recognize the constant offset.

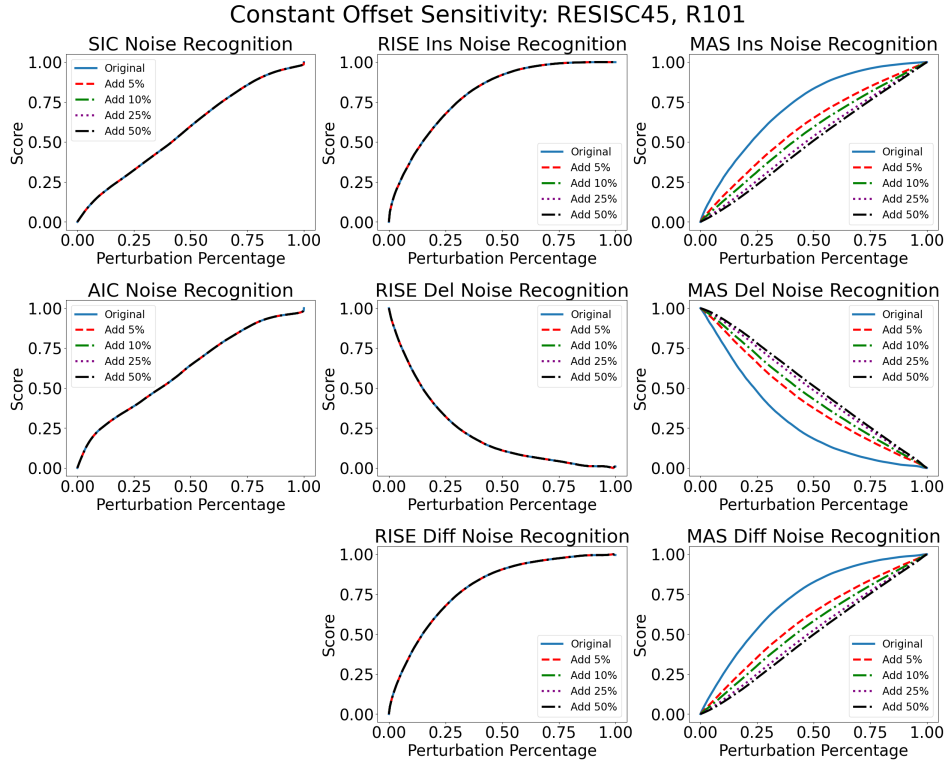


Figure 8: The ROC curves from the constant offset sensitivity test for the RESISC45 dataset and R101 model. MAC is seen to be sensitive to the constant offset, while PIC and RISE cannot recognize the constant offset.

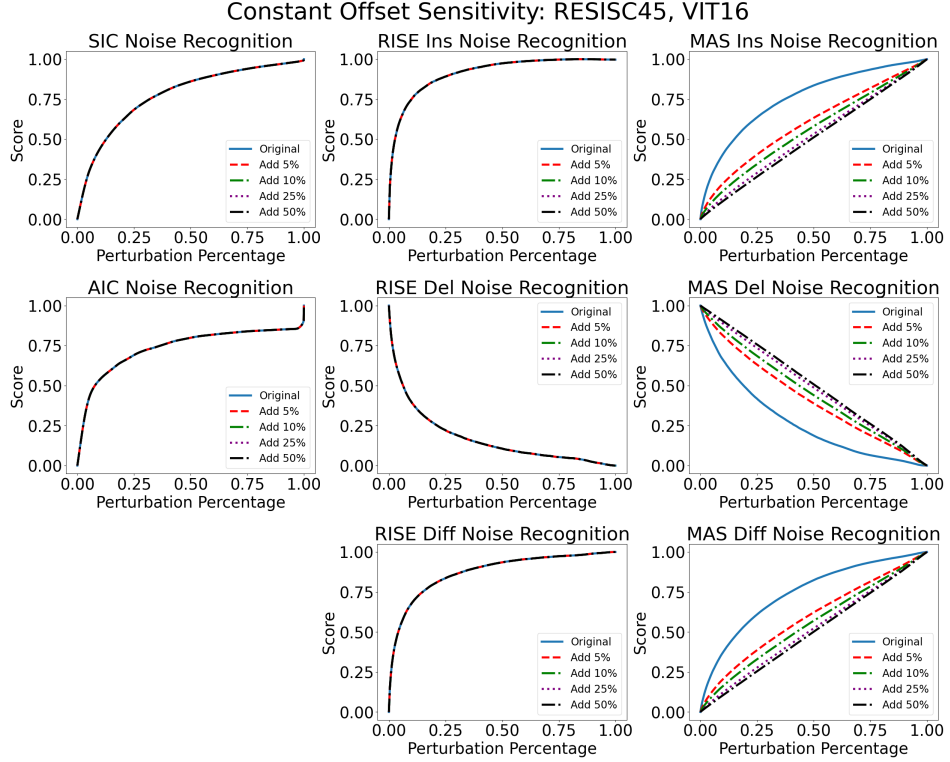


Figure 9: The ROC curves from the constant offset sensitivity test for the RESISC45 dataset and VIT16 model. MAC is seen to be sensitive to the constant offset, while PIC and RISE cannot recognize the constant offset.

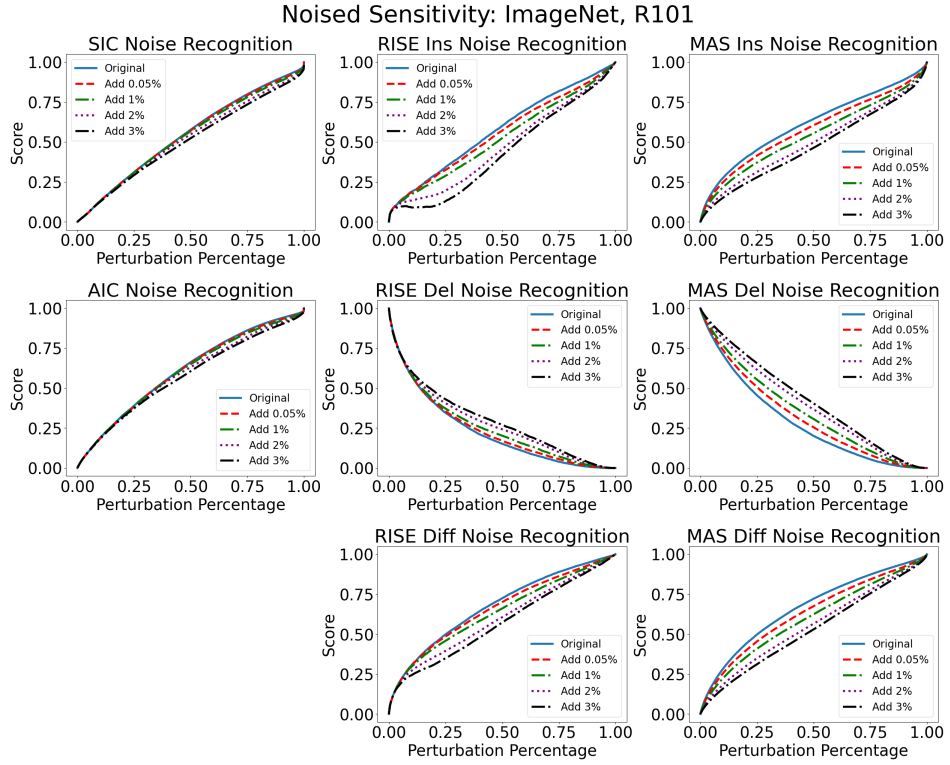


Figure 10: The ROC curves from the noised attribution sensitivity test for the ImageNet dataset and R101 model. MAC is seen to be more sensitive than PIC and RISE, while always reducing score, unlike RISE and PIC.

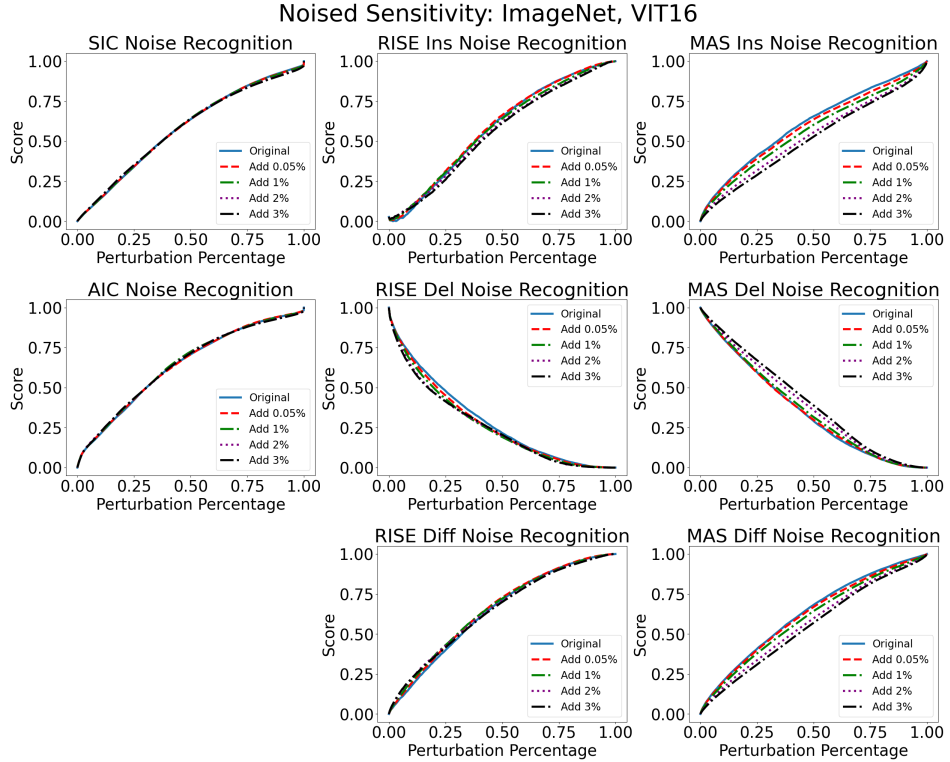


Figure 11: The ROC curves from the noised attribution sensitivity test for the ImageNet dataset and VIT16 model. MAC is seen to be more sensitive than PIC and RISE, while always reducing score, unlike RISE and PIC.

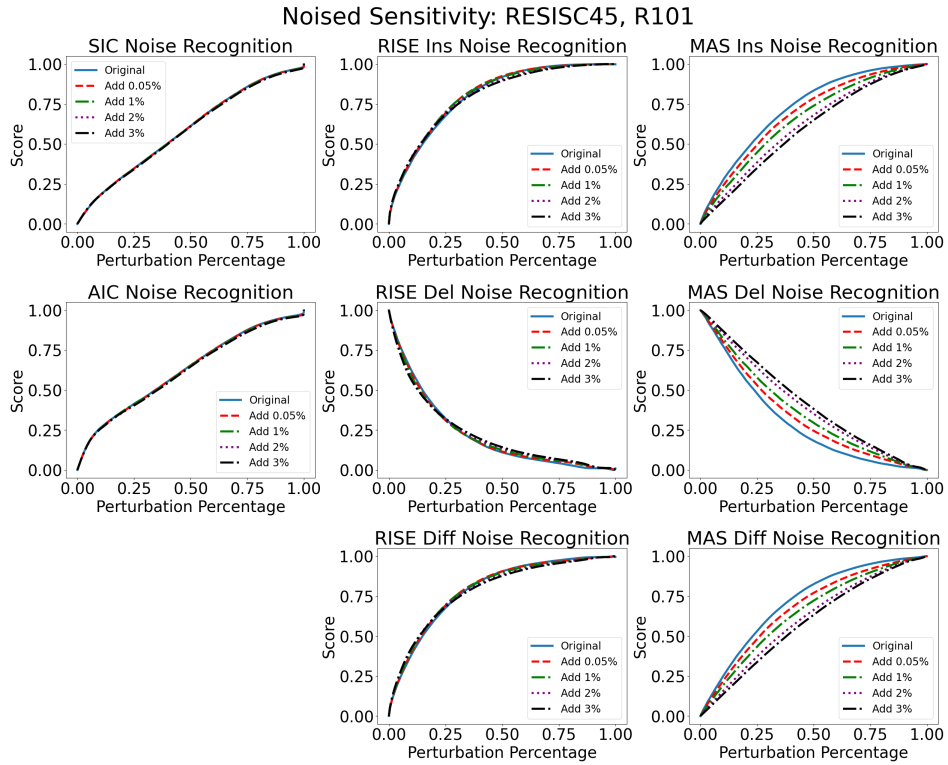


Figure 12: The ROC curves from the noised attribution sensitivity test for the RESISC45 dataset and R101 model. MAC is seen to be more sensitive than PIC and RISE, while always reducing score, unlike RISE and PIC.

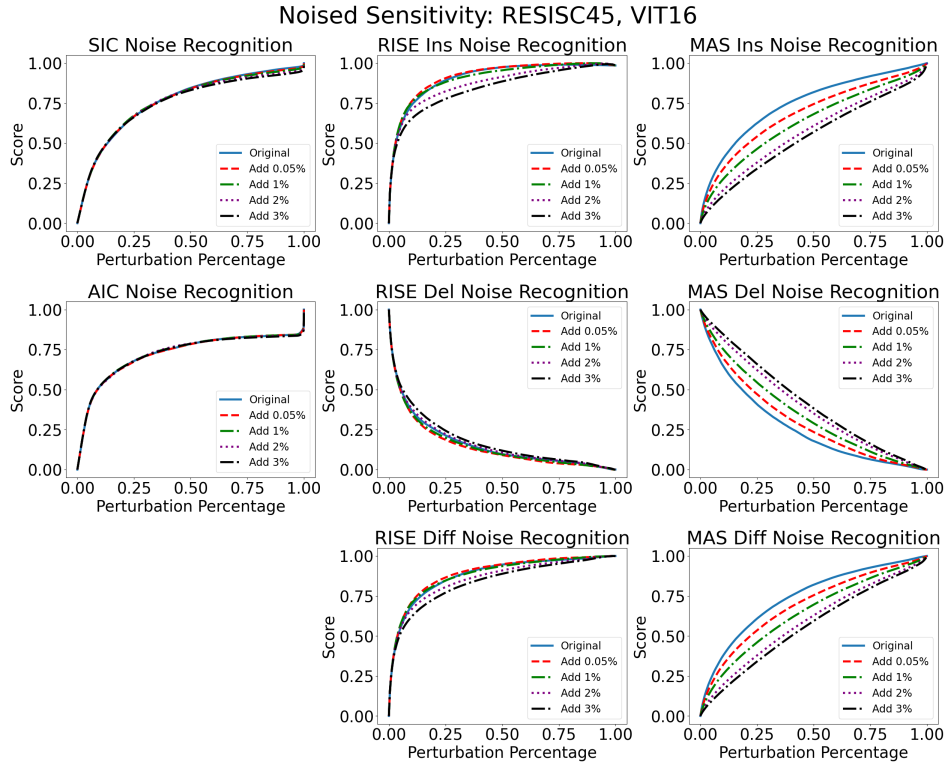
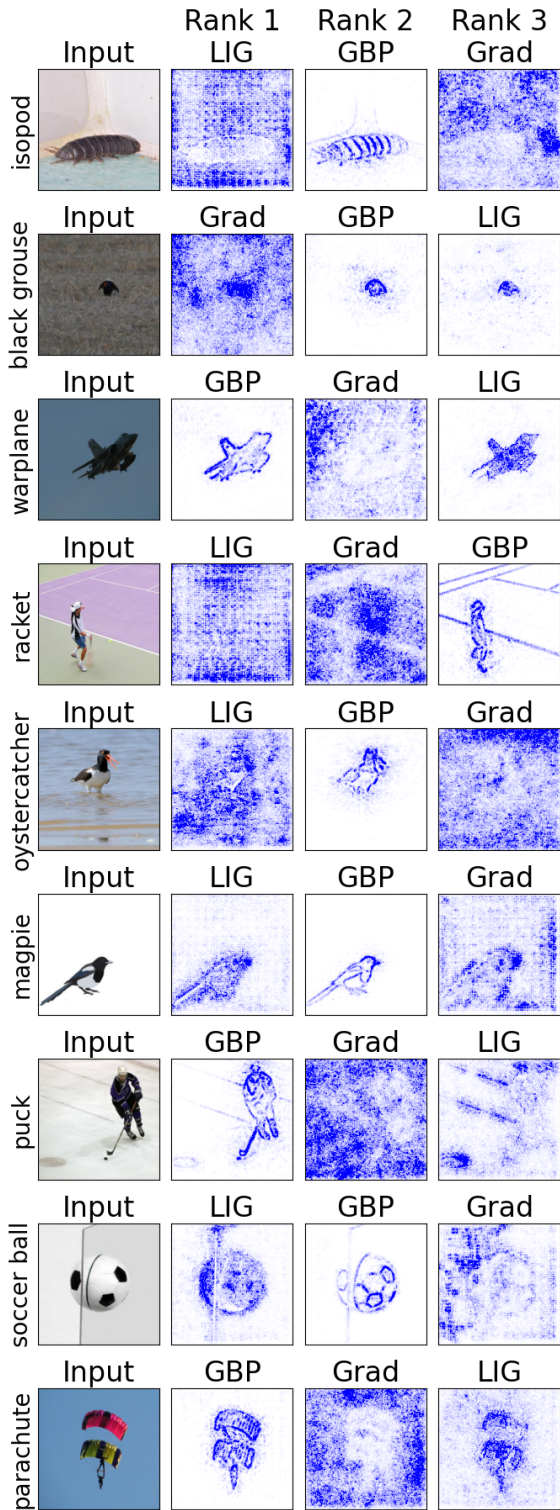


Figure 13: The ROC curves from the noised attribution sensitivity test for the RESISC45 dataset and VIT16 model. MAC is seen to be more sensitive than PIC and RISE, while always reducing score, unlike RISE and PIC.

### RISE Insertion Orderings



### MAS Insertion Orderings

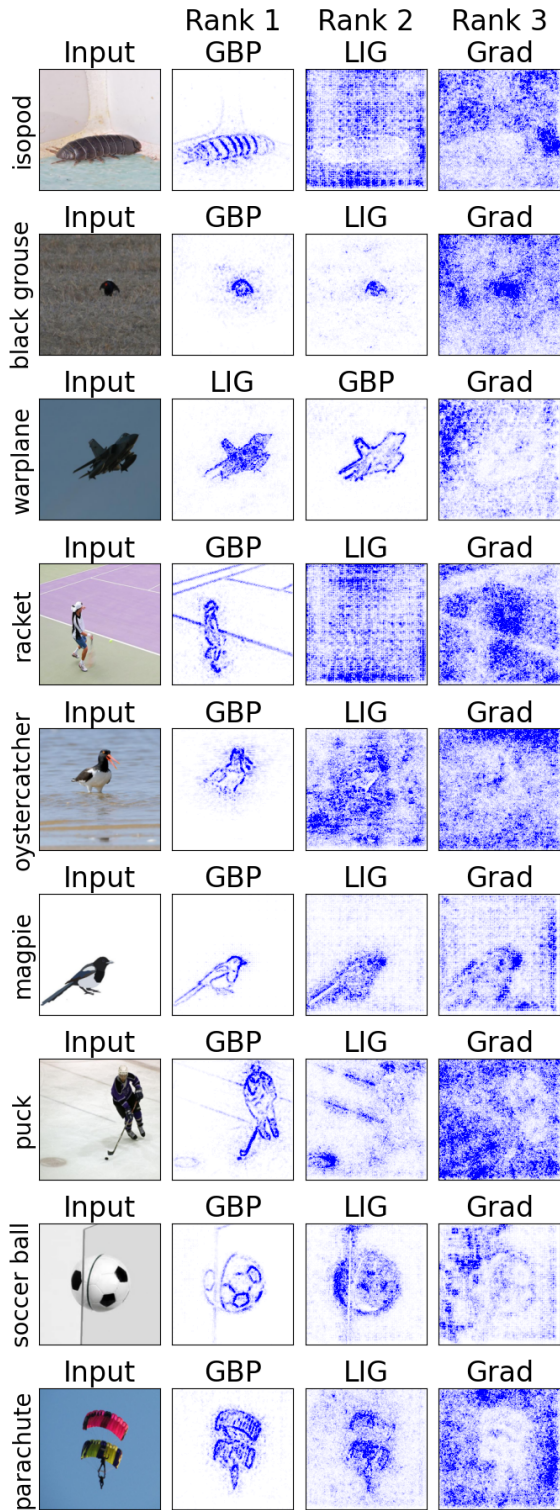


Figure 14: An illustration of the IRR consistency test. On the left, we see the ordering of attributions by RISE over a set of images where the consistency is very low across images. On the right we see the MAS ordering of the same images, which shows greatly improved consistency due to the alignment penalty that defines MAS.

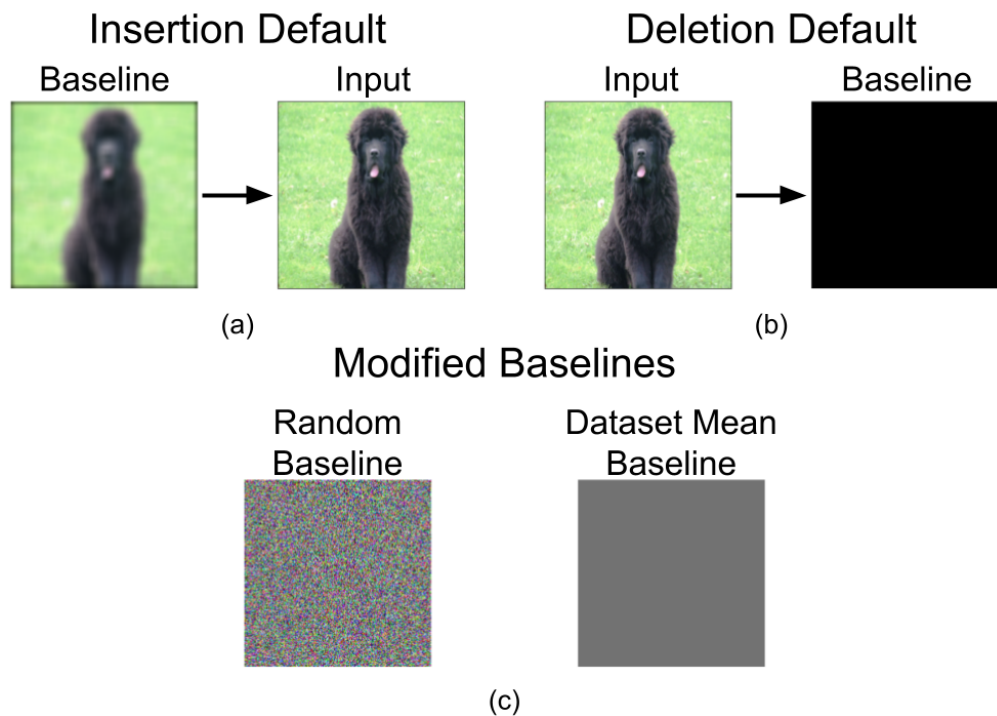


Figure 15: The default behavior of the insertion test which perturbs a blurred baseline image to the original image (a). The default behavior of the deletion test which perturbs the original image to a black baseline (b). The two modified baselines employed in the baseline invariance test: random baseline and dataset mean baseline (c).

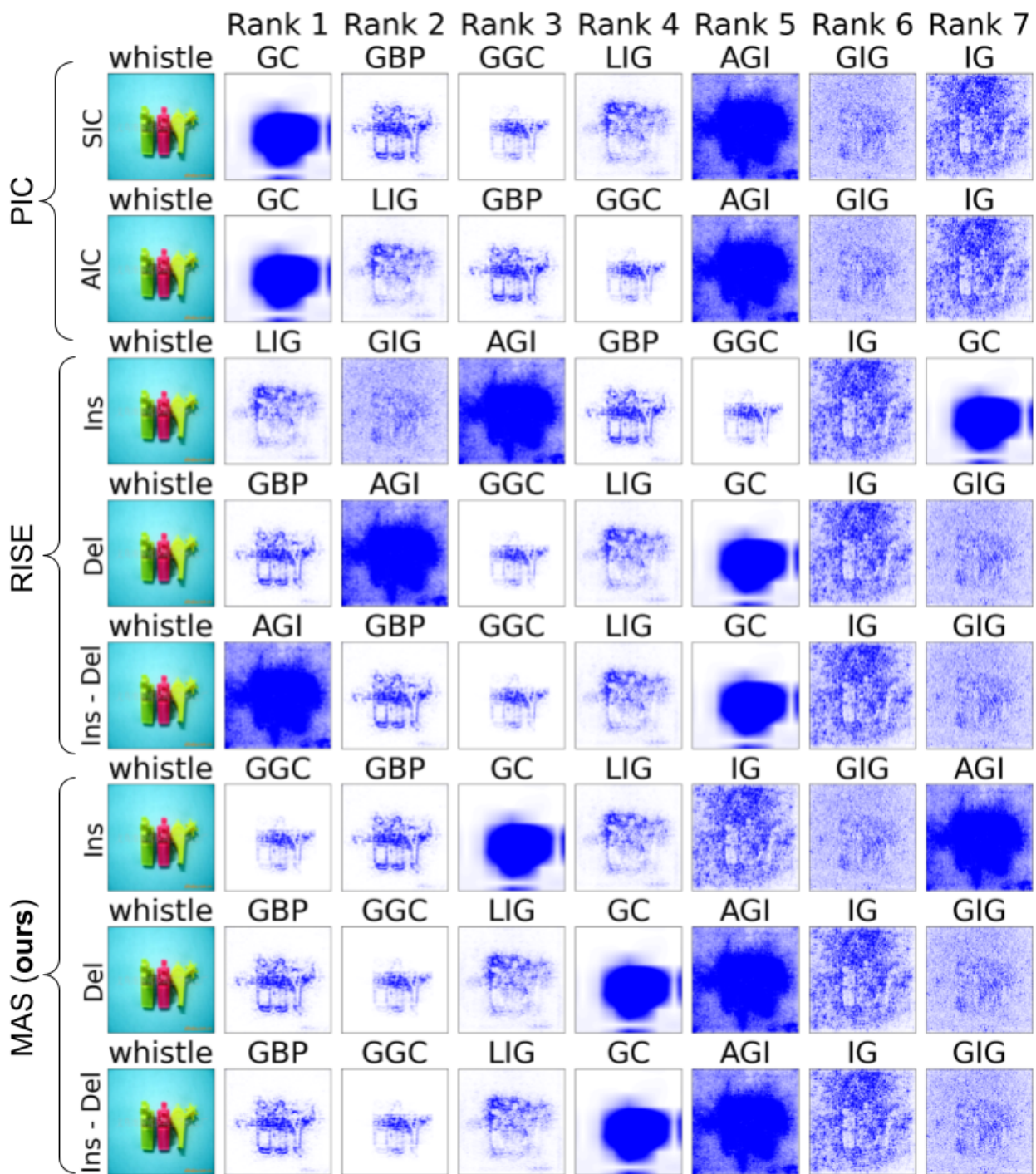


Figure 16: A consistency and sensitivity evaluation of the metrics for “whistle” attribution maps.

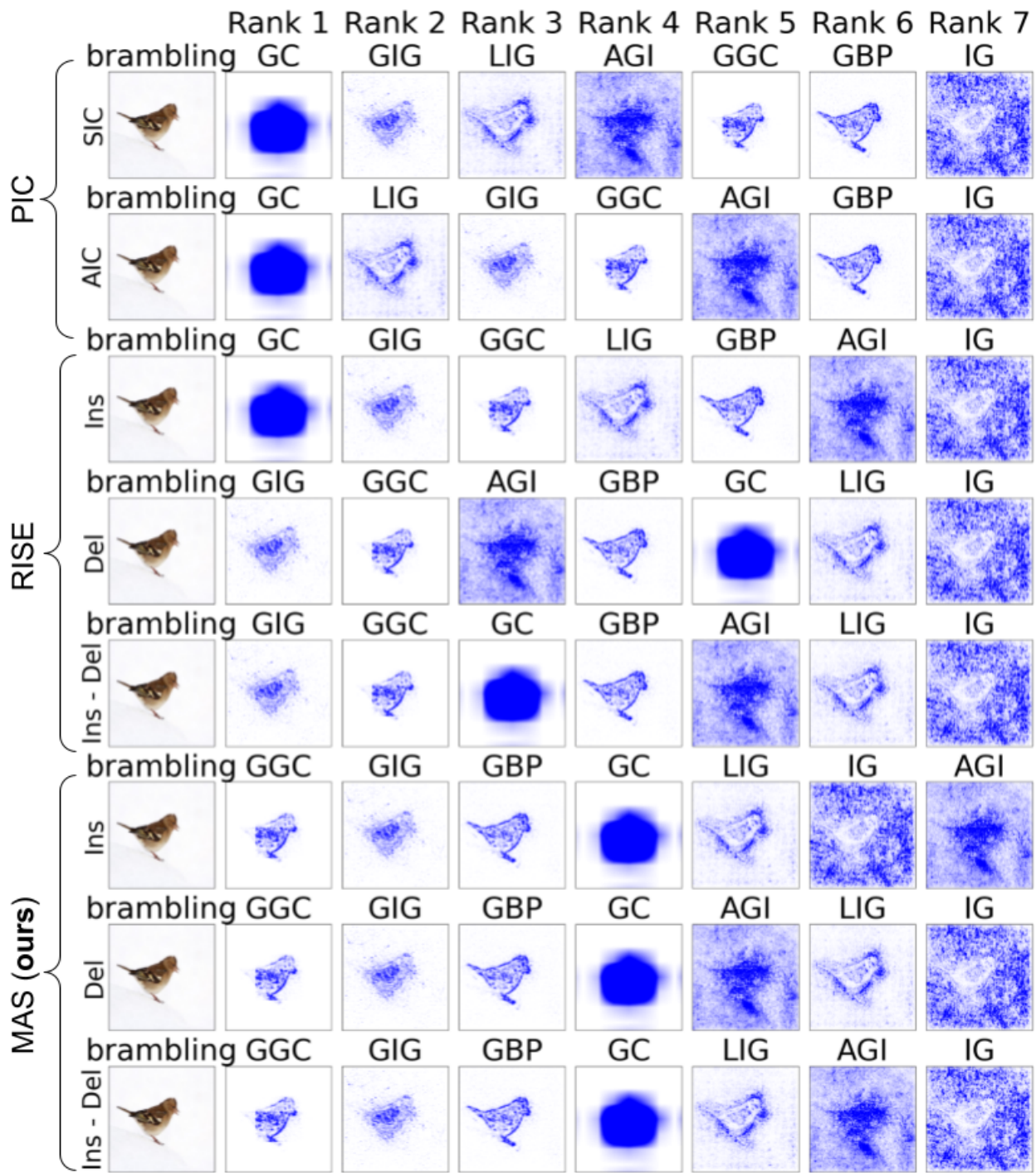


Figure 17: A consistency and sensitivity evaluation of the metrics for “brambling” attribution maps.

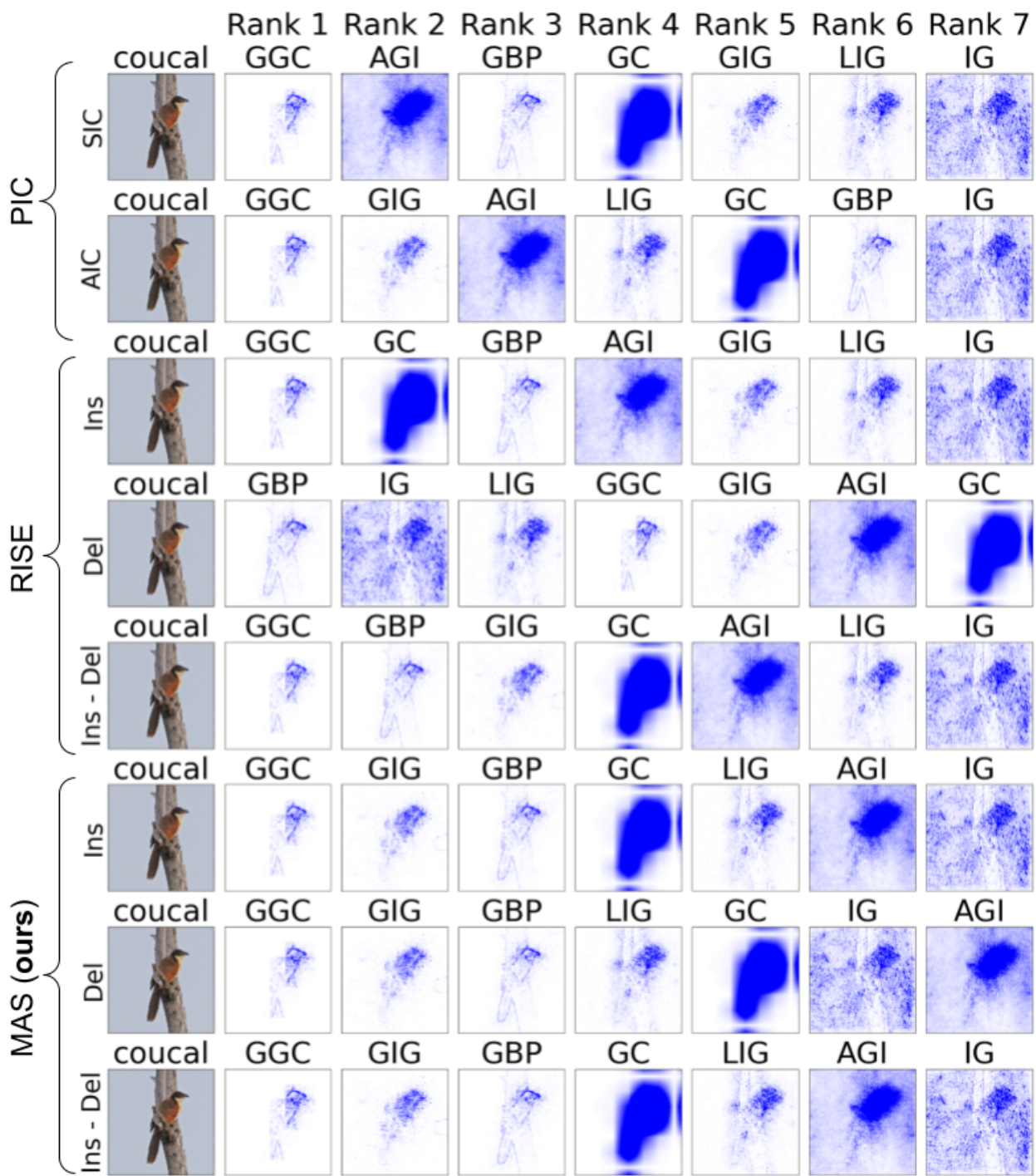


Figure 18: A consistency and sensitivity evaluation of the metrics for “coucal” attribution maps.

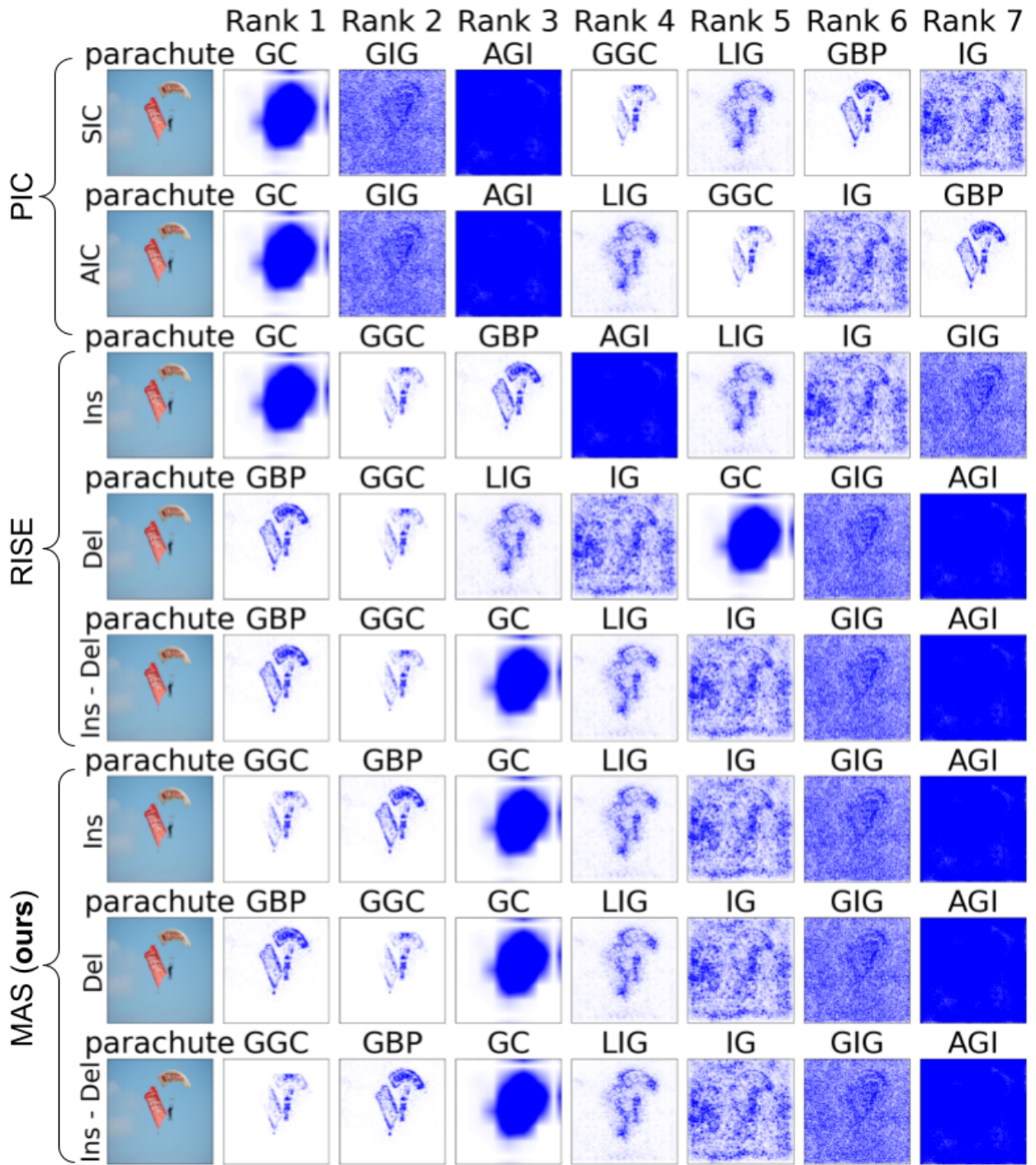


Figure 19: A consistency and sensitivity evaluation of the metrics for “parachute” attribution maps.

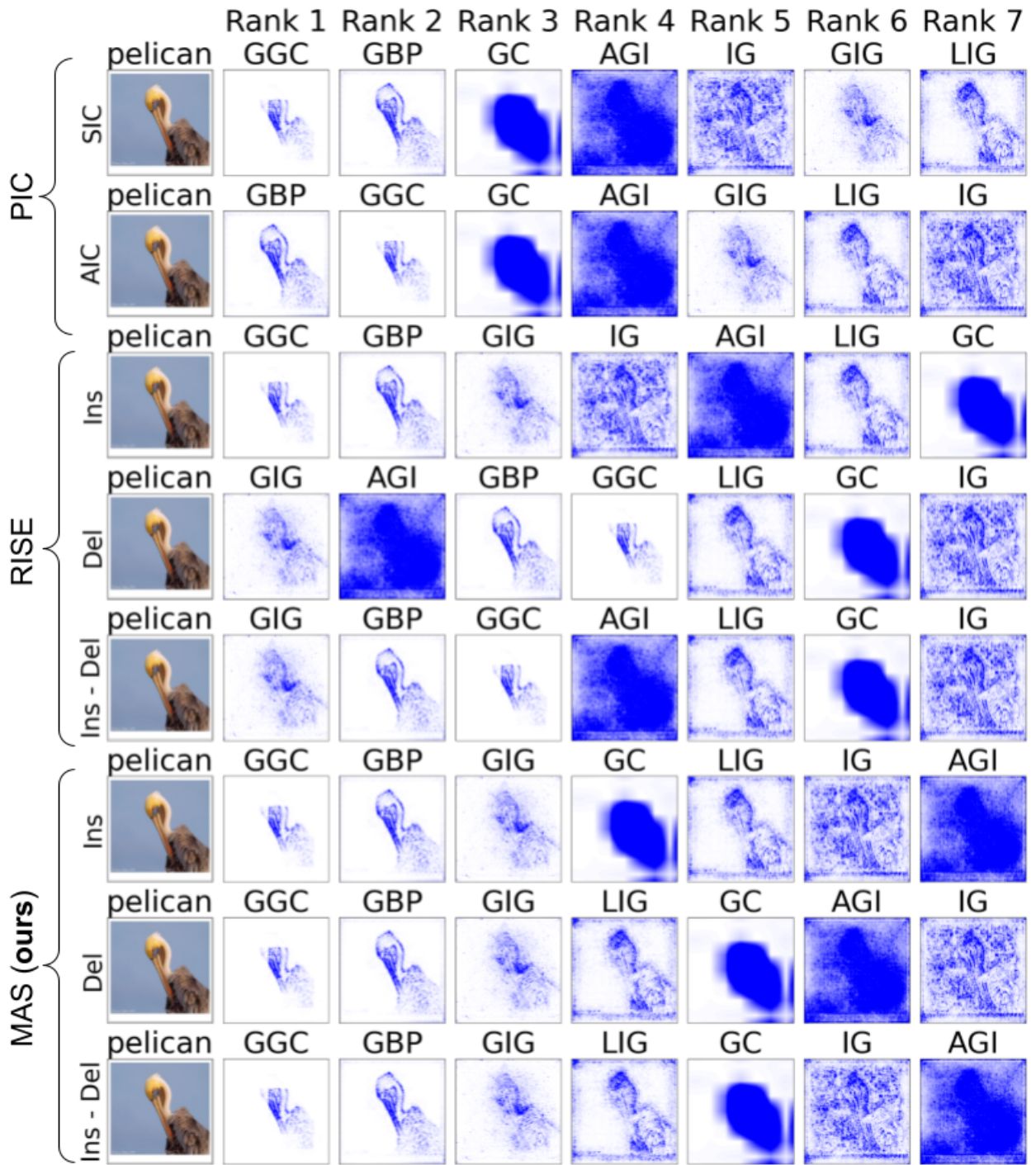


Figure 20: A consistency and sensitivity evaluation of the metrics for “pelican” attribution maps.

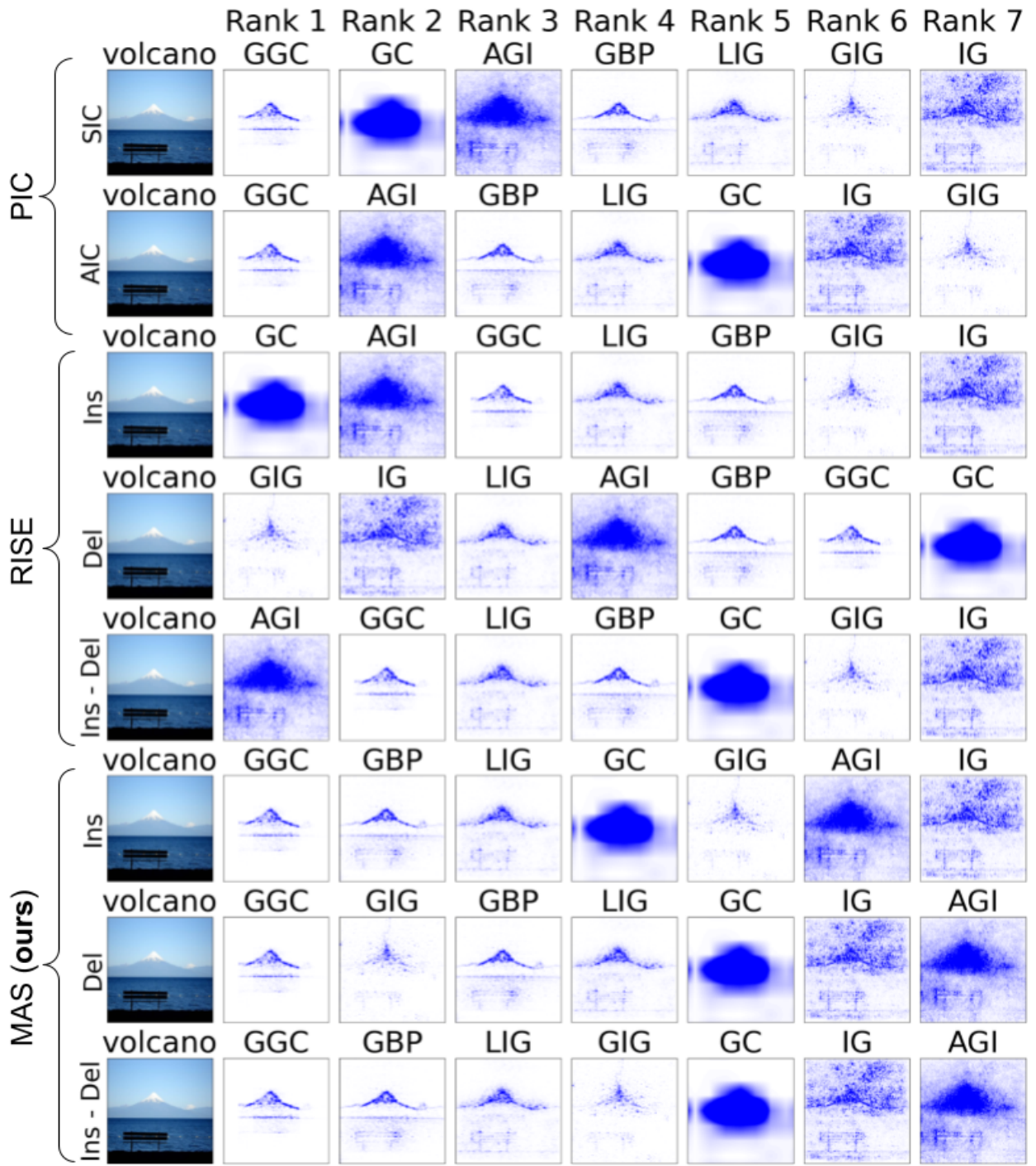


Figure 21: A consistency and sensitivity evaluation of the metrics for “volcano” attribution maps.

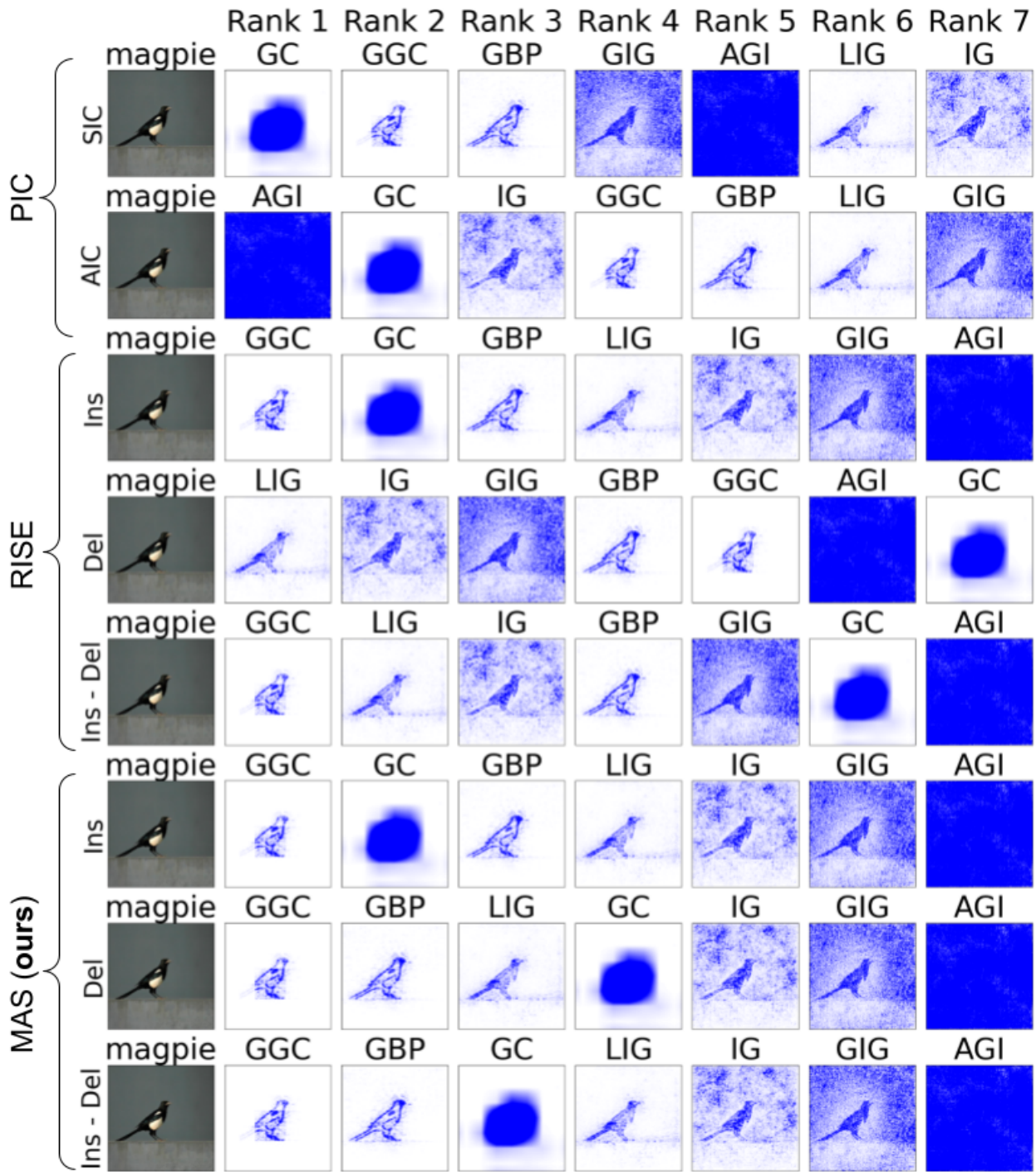


Figure 22: A consistency and sensitivity evaluation of the metrics for “magpie” attribution maps.

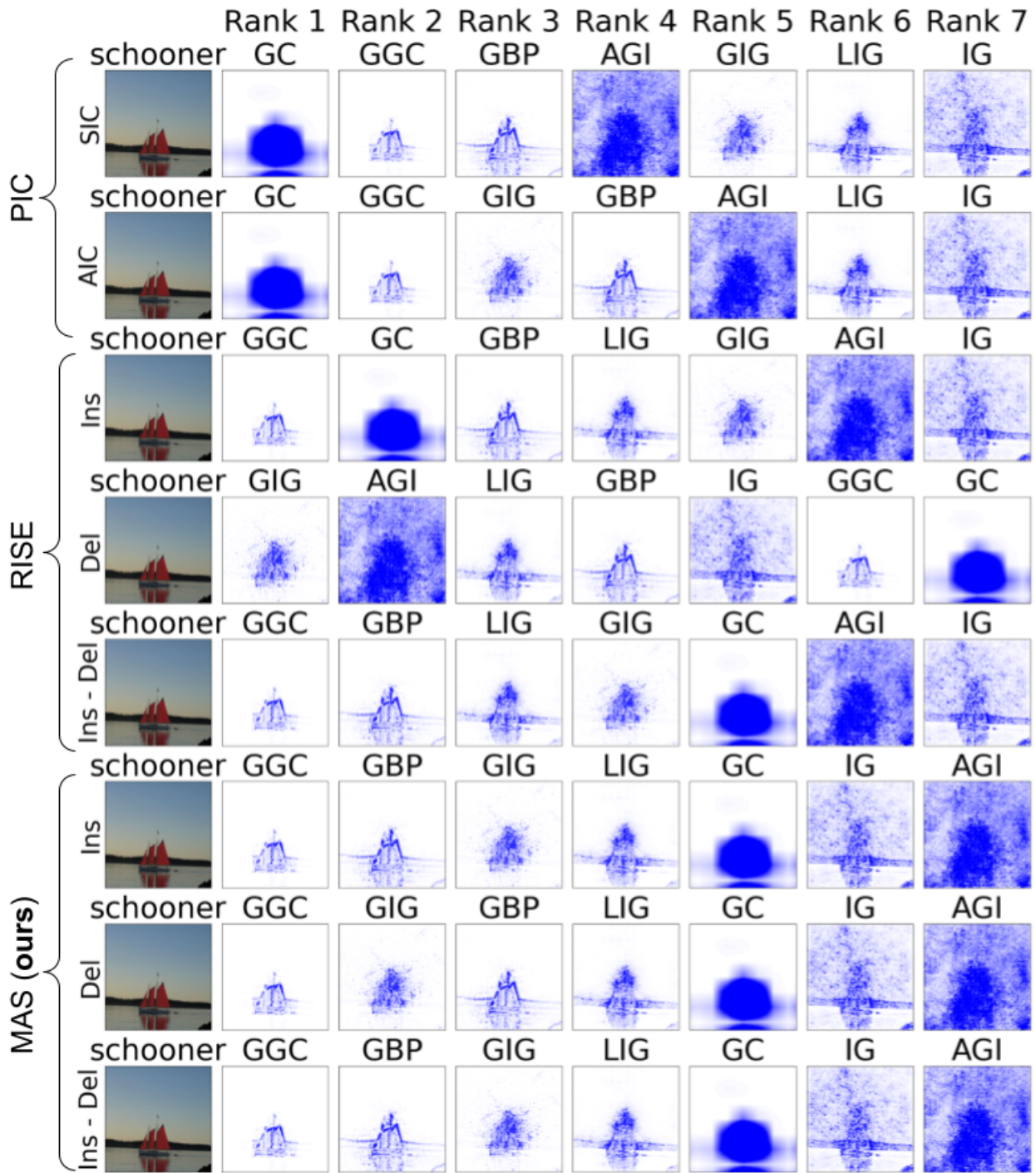


Figure 23: A consistency and sensitivity evaluation of the metrics for “schooner” attribution maps.

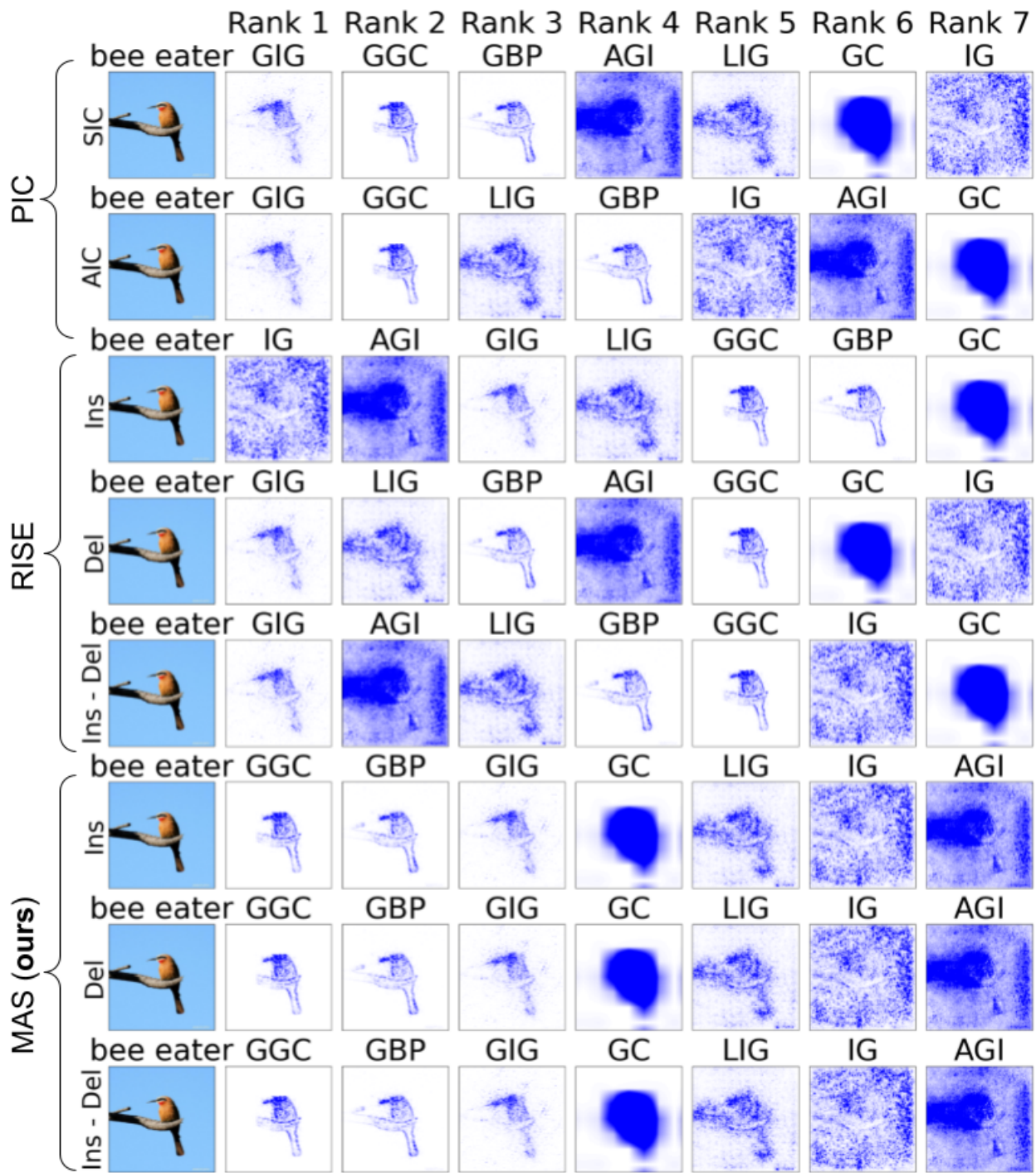


Figure 24: A consistency and sensitivity evaluation of the metrics for “bee eater” attribution maps.

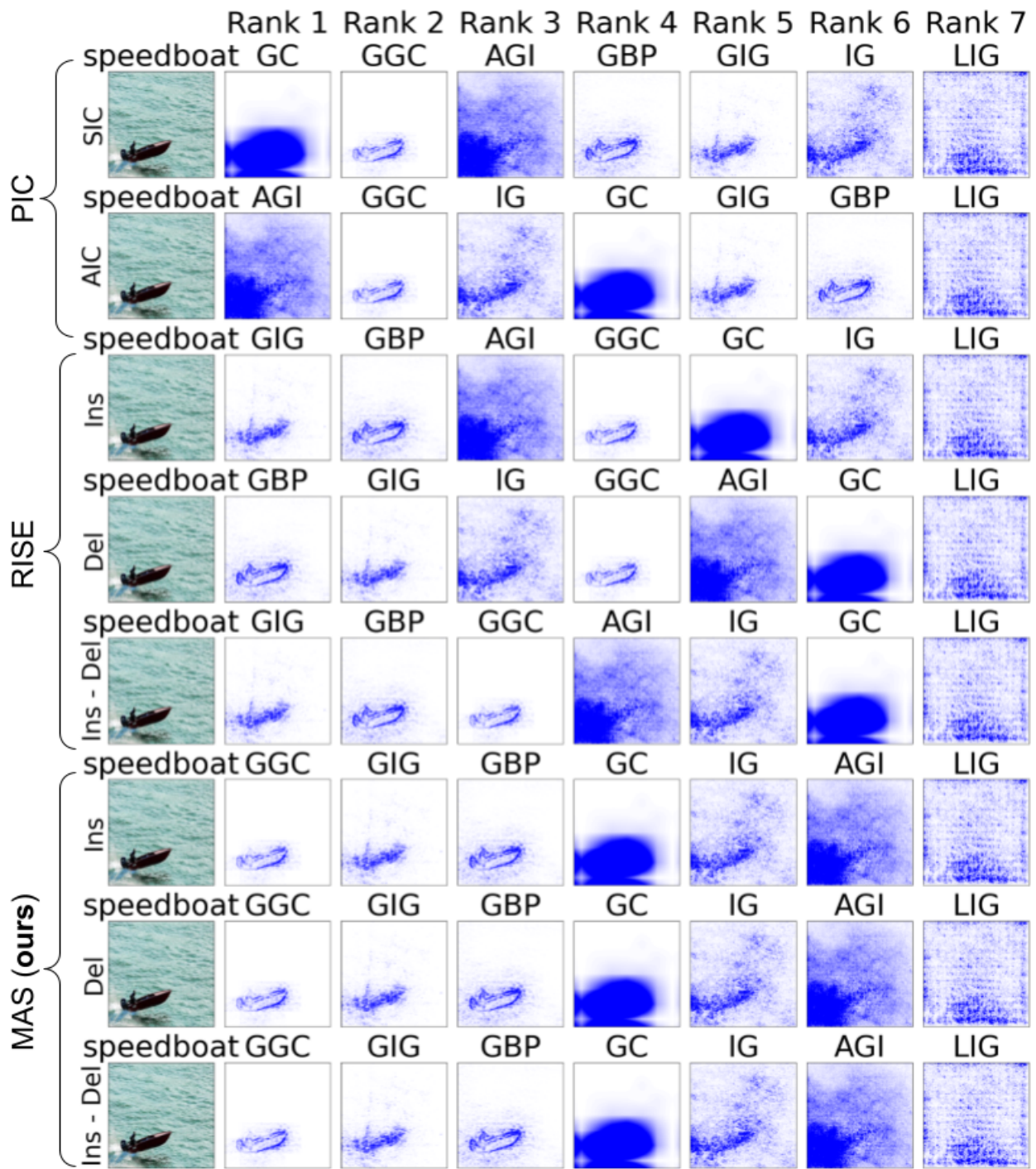


Figure 25: A consistency and sensitivity evaluation of the metrics for “speedboat” attribution maps.

## Acknowledgements

The authors were in part supported by Lockheed Martin Corporation and the Florida High Tech Corridor. This material is partially based on research sponsored by DARPA under agreement number #FA8750-23-2-0501 and #HR00112020002. This material is partially based upon work supported by the U.S. Department of Energy, Office of Science, Office of Advanced Scientific Computing Research, under Award Number #DE-SC0023494. The U.S. Government is authorized to reproduce and distribute reprints for Governmental purposes notwithstanding any copyright notation thereon. The views and conclusions contained herein are those of the authors and should not be interpreted as necessarily representing the official policies or endorsements, either expressed or implied, of DARPA, or DOE, or the U.S. Government.

## References

- [Adebayo *et al.*, 2018] Julius Adebayo, Justin Gilmer, Michael Muelly, Ian Goodfellow, Moritz Hardt, and Been Kim. Sanity checks for saliency maps. *NeurIPS*, 31, 2018.
- [Ancona *et al.*, 2018] Marco Ancona, Enea Ceolini, Cengiz Öztieli, and Markus Gross. Towards better understanding of gradient-based attribution methods for deep neural networks. In *International Conference on Learning Representations*, 2018.
- [Borji *et al.*, 2013] Ali Borji, Dicky N. Sihite, and Laurent Itti. Quantitative analysis of human-model agreement in visual saliency modeling: A comparative study. *IEEE Transactions on Image Processing*, 22(1):55–69, 2013.
- [Bylinskii *et al.*, 2019] Zoya Bylinskii, Tilke Judd, Aude Oliva, Antonio Torralba, and Frédo Durand. What do different evaluation metrics tell us about saliency models? *IEEE Transactions on Pattern Analysis and Machine Intelligence*, 41(3):740–757, 2019.
- [Chefer *et al.*, 2021] Hila Chefer, Shir Gur, and Lior Wolf. Transformer interpretability beyond attention visualization. In *Proceedings of the IEEE/CVF conference on computer vision and pattern recognition*, pages 782–791, 2021.
- [Cheng *et al.*, 2017] Gong Cheng, Junwei Han, and Xiaoliang Lu. Remote sensing image scene classification: Benchmark and state of the art. *Proceedings of the IEEE*, 105(10):1865–1883, 2017.
- [Das and Rad, 2020] Arun Das and Paul Rad. Opportunities and challenges in explainable artificial intelligence (xai): A survey, 2020.
- [Dosovitskiy *et al.*, 2020] Alexey Dosovitskiy, Lucas Beyer, Alexander Kolesnikov, Dirk Weissenborn, Xiaohua Zhai, Thomas Unterthiner, Mostafa Dehghani, Matthias Minderer, Georg Heigold, Sylvain Gelly, et al. An image is worth 16x16 words: Transformers for image recognition at scale. *arXiv preprint arXiv:2010.11929*, 2020.
- [Hao *et al.*, 2021] Yaru Hao, Li Dong, Furu Wei, and Ke Xu. Self-attention attribution: Interpreting information interactions inside transformer. In *Proceedings of the AAAI Conference on Artificial Intelligence*, volume 35, pages 12963–12971, 2021.
- [He *et al.*, 2016] Kaiming He, Xiangyu Zhang, Shaoqing Ren, and Jian Sun. Deep residual learning for image recognition. In *Proceedings of the IEEE conference on computer vision and pattern recognition*, pages 770–778, 2016.
- [Hooker *et al.*, 2019a] Sara Hooker, Dumitru Erhan, Pieter-Jan Kindermans, and Been Kim. A benchmark for interpretability methods in deep neural networks. *Advances in neural information processing systems*, 32, 2019.
- [Hooker *et al.*, 2019b] Sara Hooker, Dumitru Erhan, Pieter-Jan Kindermans, and Been Kim. A benchmark for interpretability methods in deep neural networks. *Advances in neural information processing systems*, 32, 2019.
- [Kapishnikov *et al.*, 2019] A. Kapishnikov, T. Bolukbasi, F. Viegas, and M. Terry. Xrai: Better attributions through regions. In *2019 IEEE/CVF International Conference on Computer Vision (ICCV)*, pages 4947–4956, Los Alamitos, CA, USA, nov 2019. IEEE Computer Society.
- [Kapishnikov *et al.*, 2021a] A. Kapishnikov, S. Venugopalan, B. Avci, B. Wedin, M. Terry, and T. Bolukbasi. Guided integrated gradients: an adaptive path method for removing noise. In *2021 IEEE/CVF Conference on Computer Vision and Pattern Recognition (CVPR)*, pages 5048–5056, Los Alamitos, CA, USA, jun 2021. IEEE Computer Society.
- [Kapishnikov *et al.*, 2021b] A. Kapishnikov, S. Venugopalan, B. Avci, B. Wedin, M. Terry, and T. Bolukbasi. Xrai code repository, 2021. Accessed: 2022-10-15.
- [Krippendorff, 2004] Klaus Krippendorff. *Content Analysis: An Introduction to Its Methodology (second edition)*. Sage Publications, 2004.
- [Kümmerer *et al.*, 2014] Matthias Kümmerer, Thomas Walilis, and Matthias Bethge. How close are we to understanding image-based saliency? *arXiv preprint arXiv:1409.7686*, 2014.
- [Miglani *et al.*, 2020] Vivek Miglani, Narine Kokhlikyan, Bilal Alsallakh, Miguel Martin, and Orion Reblitz-Richardson. Investigating saturation effects in integrated gradients, 2020.
- [Pan *et al.*, 2021] Deng Pan, Xin Li, and Dongxiao Zhu. Explaining deep neural network models with adversarial gradient integration. In Zhi-Hua Zhou, editor, *Proceedings of the Thirtieth International Joint Conference on Artificial Intelligence, IJCAI-21*, pages 2876–2883. International Joint Conferences on Artificial Intelligence Organization, 8 2021. Main Track.
- [Paszke *et al.*, 2019] Adam Paszke, Sam Gross, Francisco Massa, Adam Lerer, James Bradbury, Gregory Chanan, Trevor Killeen, Zeming Lin, Natalia Gimelshein, Luca Antiga, Alban Desmaison, Andreas Köpf, Edward Yang, Zach DeVito, Martin Raison, Alykhan Tejani, Sasank Chilamkurthy, Benoit Steiner, Lu Fang, Junjie Bai, and Soumith Chintala. Pytorch: An imperative style, high-performance deep learning library. In *Proceedings of the*

- [33rd International Conference on Neural Information Processing Systems. Curran Associates Inc., 2019.]
- [Petsiuk *et al.*, 2018a] Vitali Petsiuk, Abir Das, and Kate Saenko. Rise code repository, 2018. Accessed: 2022-11-01.
- [Petsiuk *et al.*, 2018b] Vitali Petsiuk, Abir Das, and Kate Saenko. Rise: Randomized input sampling for explanation of black-box models. In *Proceedings of the British Machine Vision Conference (BMVC)*, 2018.
- [Qiang *et al.*, 2022] Yao Qiang, Deng Pan, Chengyin Li, Xin Li, Rhongho Jang, and Dongxiao Zhu. Attcat: Explaining transformers via attentive class activation tokens. In S. Koyejo, S. Mohamed, A. Agarwal, D. Belgrave, K. Cho, and A. Oh, editors, *Advances in Neural Information Processing Systems*, volume 35, pages 5052–5064. Curran Associates, Inc., 2022.
- [Ribeiro *et al.*, 2016] Marco Tulio Ribeiro, Sameer Singh, and Carlos Guestrin. “why should i trust you?” explaining the predictions of any classifier. In *Proceedings of the 22nd ACM SIGKDD international conference on knowledge discovery and data mining*, pages 1135–1144, 2016.
- [Russakovsky *et al.*, 2015] Olga Russakovsky, Jia Deng, Hao Su, Jonathan Krause, Sanjeev Satheesh, Sean Ma, Zhiheng Huang, Andrej Karpathy, Aditya Khosla, Michael Bernstein, Alexander C. Berg, and Li Fei-Fei. ImageNet Large Scale Visual Recognition Challenge. *International Journal of Computer Vision (IJCV)*, 115(3):211–252, 2015.
- [Samek *et al.*, 2016] Wojciech Samek, Alexander Binder, Grégoire Montavon, Sebastian Lapuschkin, and Klaus-Robert Müller. Evaluating the visualization of what a deep neural network has learned. *IEEE transactions on neural networks and learning systems*, 28(11):2660–2673, 2016.
- [Selvaraju *et al.*, 2017] Ramprasaath R Selvaraju, Michael Cogswell, Abhishek Das, Ramakrishna Vedantam, Devi Parikh, and Dhruv Batra. Grad-cam: Visual explanations from deep networks via gradient-based localization. In *Proceedings of the IEEE international conference on computer vision*, pages 618–626, 2017.
- [Shrikumar *et al.*, 2016] Avanti Shrikumar, Peyton Greenside, Anna Shcherbina, and Anshul Kundaje. Not just a black box: Learning important features through propagating activation differences. *arXiv preprint arXiv:1605.01713*, 2016.
- [Simonyan *et al.*, 2014] Karen Simonyan, Andrea Vedaldi, and Andrew Zisserman. Deep inside convolutional networks: Visualising image classification models and saliency maps, 2014.
- [Springenberg *et al.*, 2015] Jost Tobias Springenberg, Alexey Dosovitskiy, Thomas Brox, and Martin Riedmiller. Striving for simplicity: The all convolutional net, 2015.
- [Sundararajan *et al.*, 2017] Mukund Sundararajan, Ankur Taly, and Qiqi Yan. Axiomatic attribution for deep networks. In *Proceedings of the 34th International Conference on Machine Learning - Volume 70*, ICML’17, page 3319–3328. JMLR.org, 2017.
- [Tomsett *et al.*, 2020] Richard Tomsett, Dan Harborne, Supriyo Chakraborty, Prudhvi Gurram, and Alun Preece. Sanity checks for saliency metrics. In *AAAI*, volume 34, pages 6021–6029, 2020.
- [Yuan *et al.*, 2021] Tingyi Yuan, Xuhong Li, Haoyi Xiong, Hui Cao, and Dejing Dou. Explaining information flow inside vision transformers using markov chain. In *eXplainable AI approaches for debugging and diagnosis.*, 2021.
- [Zeiler and Fergus, 2014] Matthew D Zeiler and Rob Fergus. Visualizing and understanding convolutional networks. In *European conference on computer vision*, pages 818–833. Springer, 2014.